Translated from *Uspekhi Khimii* **61** 734–764 (1992) U.D.C. 541.138

Electrochemistry of transition metal single crystals with well defined surfaces

G V Khaldeev, T A Syur
Gor'kii Perm' State University

ABSTRACT. The effect of extended defects of the surface of metallic single crystals on the electrochemical processes of dissolution and formation of a new phase has been analysed. Theoretical ideas on the rearrangement of a crystal surface (phase transitions of the second kind) during the adsorption of surface-active substances are presented. The reconstruction (faceting) of the surface under the influence of electrochemical processes and the adsorption of nucleophilic species (hydrogen, oxygen, halogen ions) from the gas phase and from electrolytes on a well defined metal single crystal surface have been evaluated.

The bibliography contains 94 references.

Contents

I. Introduction 399
II. Surface defects. The discrete metal lattice model 399
III. Orientation dependence of the dissolution of a metal during phase transitions of the first kind (corrosion, electrocrystallisation) 400
IV. Adsorption of chalcophilic particles and phase transitions of the second kind in the near-surface layers of monocrystals. 402
V. Reconstruction of monocrystal surfaces during the adsorption of hydrogen, oxygen, and halogens 404
VI. Conclusions 415

I. Introduction

Expermental studies of the electrochemistry of well defined metal single crystal surfaces have stimulated the development of new theoretical models. The use of methods having a local resolution better than 0.1 nm provides information on the reconstruction of near-surface layers of the crystal, which usually have a stepped structure with a range of surface-active centres.

The flat condenser model (the boundary between an infinite defect-free crystal and an isotropic liquid medium) does not give a strictly quantitative description of the mechanism of the electrochemical corrosion process. The metal surface (M) contains surface defects which create adsorption centres of various types and which have different energy levels. These centres generate fields associated with deformation displacements. The description of the discrete structure of the interface must allow for the formation of complex electrical double layers (EDL) on both the metal and the electrolyte side: electrons from the metal penetrate into the active part of the fixed EDL forming electron tails. The components of the electrolyte adsorbed on the metal experience the action of the electron tails; this produces long-range order in the film, which acquires a quasi-crystalline structure.[1]

In this review we shall examine recently published data on the effect of the reconstruction of the first few near-surface layers by the adsorption-chemical interaction with the electrolyte particles upon the conditions of formation of a new phase during an electrochemical process. Often the interaction on an M/electrolyte interface does not produce a phase transition of the first kind (corrosion) but is limited to a transition of the second kind which changes the short-range order of the hierarchical structures of the EDL both in the electrolyte and in the metal. Unfortunately only a few electrochemists have paid sufficient attention to the characterisation of the surface and to the analysis of changes in the structure of near-surface layers of monocrystalline samples. Our analysis of experimental information on crystal surfaces must therefore be limited to data for surfaces having reliably determined crystallographic characteristics.

II. Surface defects. The discrete metal lattice model

The first model to succeed the parallel plate condenser model was the "jelly" model, in which the near-surface layer consists of an ensemble of uniformly charged spherically symmetrical atoms. Each pair of atoms in the first near-surface layer was characterised by a defined binding energy E_b, decreasing with increasing distance (r_{ij}) between the atoms. Because of the periodicity of the structure of a metallic crystal the E_b values are crystallographically related, and periodic bond chains (PBC) can be delineated in the first near-surface layers.

According to the generally adopted Franck–Cabrera classification[2] solid surfaces are divided into singular, near-singular (vicinal), and non-singular (diffuse), usually called *F*, *S*, and *K* faces. The *F* faces are the surfaces parallel to the two PBC systems with the largest E_b. Atomically smooth singular surfaces coincide with the low-index crystallographic planes and have a different packing density S_{hkl} of the surface atoms. The atomically rough (slightly inclined to the *F* faces) vicinal *S* faces deviate by a small angle from the singular orientation and have a stepped structure (Table 1): the length *L* exceeds the height *h* of the steps (low-index planes). The vicinal *S* faces can be stabilised by the reconstruction of the terraces between the steps. This has been observed expermentally for planes close to (100) and (111) in Au.[4] At certain "magic" angles, defining the deviation of (*khl*) from the low-index face, and for which the distances between steps are multiples of the period of the superstructure, the energy of the surface is substantially decreased.[5] Surfaces with different orientations, characterised by large step heights (β_0), are non-singular *K* faces (in which the step length *L* is

commensurate with the step height h). Examples of stepped surfaces of the $n(110)-(0\bar{1}1)-(0\bar{1}1)$, $n(110)-(1\bar{1}0)$, and $n(110)-(001)$ type are shown in Fig. 1 (where n is the number of rows of atoms in the terrace).

Table 1. Types of stepped surface (S faces) in the cubic system.[8]

Symbol of the stepped face	Miller indices	Angles between flat terraces and steps
$n(111)-(111)$	$(n, n, n-2)$	$\mathrm{tg}^{-1}\left(\frac{2\sqrt{2}}{3n-2}\right)$
Sample: 9(111)–(111)	(997)	6.45°
$n(111)-(100)$	$(n+1, n-1, n-1)$	$\mathrm{tg}^{-1}\left(\frac{2\sqrt{2}}{3n-1}\right)$
Sample: 10(111)–(100)	(11, 9, 9)	5.57°
$n(100)-(111)$	$(2n-1, 1, 1)$	$\mathrm{tg}^{-1}\left(\frac{\sqrt{2}}{2n-1}\right)$
Sample: 10(100)–(111)	(19, 1, 1)	4.25°
$n(100)-(110)$	$(n, 1, 0)$	$\mathrm{tg}^{-1}\left(\frac{1}{n}\right)$
Sample: 9(100)–(110)	(910)	6.34°
$n(110)-(111)$	$(2n-1, 2n-1, 1)$	$\mathrm{tg}^{-1}\left(\frac{\sqrt{2}}{2(2n-1)}\right)$
Sample: 5(110)–(111)	(991)	4.49°
$n(110)-(100)$	$(n, n-1, 0)$	$\mathrm{tg}^{-1}\left(\frac{1}{2n-1}\right)$
Sample: 9(110)–(100)	(980)	3.37°

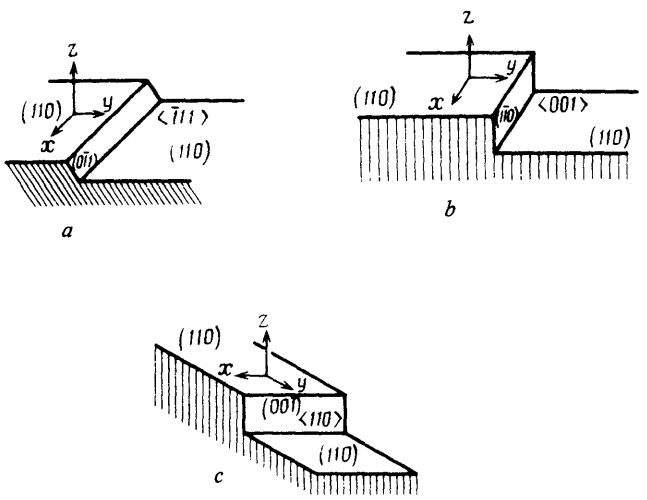


Figure 1. Geometry of the stepped surfaces; *a*, $n(110)-(0\bar{1}1)$; *b*, $n(110)-(1\bar{1}0)$; *c*, $n(110)-(001)$; n is the number of atomic rows in the terrace.

Singular surfaces have sites of a single type for capturing adsorbed species, but both one-centre adsorption and stronger multicentre adsorption can take place. According to Horiuti[6] the latter are called s states and the one-centre adsorption centres are called r states. For cubic crystals the width (r_{hkl}) and the depth (h_{hkl}) of the strong adsorption centres (s states) are calculated by the formula

$$r_{110} = a/2 - R_M,\ h_{110} = a\sqrt{2}/2 - R_M, \quad (1)$$

$$r_{100} = a\sqrt{2}/2 - R_M,\ h_{100} = a/2 - R_M, \quad (2)$$

$$r_{111} = (a/\sqrt{2})/2 \cos 30° - R_M,\ h_{111} = a\cos(\widehat{[100][111]}) - R_M, \quad (3)$$

where a is the lattice parameter of M, and R_M is the radius of the M atom, which corresponds most closely to the Zacharaisen radius $R_{M,z}$. The latter is calculated by the model of the ideal h.c.p. structure constructed from spherically symmetrical elements of radius $R_{M,z} = \Omega^{1/3}/2^{5/6}$, where Ω is the atomic volume of M at room temperature.[7]

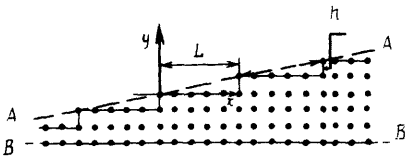


Figure 2. Square lattice with an $[lk]$ ($k = 5$) surface;[8] L is the length of the step, h is its height.

Atomically flat ideal singular F faces of M contain regular defects of the broken bond type having densities (for example, in the diamond lattice) of $\sqrt{3}/4a^2$ for the (111) face, $3/4a_2$ for the (001) face, and $3\sqrt{2}/8a^2$ for the (011) face. A simple square lattice with a single index [like the $\{lk\}$, $k = 5$ lattice surface shown in Fig. 2] is usually stepped with a step height h. Planes with the smallest number of broken bonds are energetially the most favourable for the formation of the equilibrium forms of crystals during dissolution (or corrosion). Therefore the morphology of the surface corresponds to the direction of the corrosion process which lowers the total surface energy of the system.[8]

The packing densities of the atoms are different for different S_{hkl} surfaces. Thus, the low-index (111), (001), and (011) faces of nickel crystals contain the following numbers of surface atoms (N_s) per 1 m^2 of surface area; 1.87×10^{19}, 1.61×10^{19}, and 1.14×10^{19}, and those of silver monocrystals 1.38×10^{19}, 1.20×10^{19}, and 0.84×10^{19}. Calculations of the packing densities show that the nonsingular terraced faces have the loosest surfaces. These faces, with a well defined angle of deviation from the low-index faces, are most often met in the surfaces of polycrystals.

III. Orientation dependence of the dissolution of a metal during phase transitions of the first kind (corrosion, electrocrystallisation)

Unfortunately, reliable experimental data are few, because in most cases experimental electrochemists have used monocrystals with S faces while claiming them to be singular low-index F faces. Working

surfaces are usually prepared by cutting the monocrystal by the spark erosion method, which produces the required *hkl* orientation to within $1-3°$: the working surfaces are therefore invariably stepped. The best surfaces, closest to the low-index *F* faces, have a deviation of $\sim 1°$ in the noble meals. A slight improvement can be achieved[9] by including a final ion etching stage (Ar^+) in the surface preparation programme (mechanical polishing with diamond pastes, electropolishing, chemical polishing). Clavilier and co-workers[10] used a special sample preparation programme in their electrochemical investigation, including a surface cleaning stage by vacuum annealing and cooling, and they claim a precision of $1-3'$ in their control of *hkl*.

Another weakness of many experimental studies is a casual approach to the preparation of the electrode and to the general experimental technique; oxides, adsorbed particles, and other contaminants are removed carelessly from the surface, and mechanical lapping and polishing methods are used though they are known to perturb the structure of the near-surface layer. The most reliable electrochemical data were obtained on the equilibrium faces of single-crystal whiskers, whose working *F* faces are very close to singular surfaces.

The physical methods used to characterise and to control experimentally the surface *ex situ* and *in situ* include X-ray diffraction (XRD), high-energy and low-energy electron diffraction (HEED and LEED), secondary ion mass spectroscopy (SIMS), Auger electron spectroscopy (AES), X-ray and ultraviolet photoelectron spectroscopy (XPS and UPS), elastic and inelastic neutron scattering (ENS and INS), elastic and inelastic scattering of helium atoms (EHS and IHS), and electron beam microanalysis (EBMA),[11] as well as other methods. Further developments in high-resolution electron microscopy (0.1—0.3 nm) have been achieved, with chemical analysis of the near-surface layer and new methods of exploiting the resonant scattering of X-rays[12] in interpreting the fine structure of the extended X-ray absorption spectra (EXAFS). By using these methods the distance between the absorbing atom and the atoms of the first coordination sphere can be determined to within 0.001 nm, and to within 0.01 nm for the next three spheres. Information on the local chemical composition and on the atomic and electronic structure of the surface is important for determining the electrochemical characteristics of metals. Auger electron spectroscopy can be used to calculate (from the energy of the Auger electrons) the local density of states in the valence band for the M surface. Several of the methods listed above are usually combined within the same experiment. The analytical possibilities of the methods are summarised in Table 2.

The interactive combination of these methods with electrochemical methods, which allow the degree of excitation of the particles in the near-surface layers of the metal and of the electrolyte to be controlled, makes it possible to re-examine the phase transitions of the first and second kind in the metal corrosion process and in the deposition of a new phase on the surface. The phase transition of the first kind during the dissolution of the crystal is preceded by a relaxation and rearrangement of the surface layers (phase transition of the second kind).

The dissolution of the crystal leads to the disappearance of some faces and the retention of others; in the surface layers of polycrystals the grains contacting the solution in given orientations dissolve fastest. The crystal in the solvent medium behaves so as to retain its mass by rearrangement of the near-surface layer, and the surface tension γ_{ji}^0 decreases according to the expression

$$\partial\gamma_{ij}^0/\partial r_{ij} = 0, \qquad (4)$$

where r_{ij} is the distance between interacting particles.

The positions of the individual atoms in the near-surface layer of M are jointly described by the index (*hkl*). Sites for the adsorption of surface-active substances are considered to be equivalent. The expression (4) reflects the decrease in the area of the solid surface, which must be accompanied by an increased chemical resistance of the metallic crystal in the liquid medium. The decrease in the true area of the electrode surface is reflected by the decrease in the rate of corrosion (K) as the dissolution time increases. K can be increased by special methods (stirring, the application of an anodic potential), but the maximum rate (observed at the beginning of the dissolution

Table 2. Characteristics of the different methods of studying the surface and near-surface layers of metals.[11]

Parameter	UPS	XPS	AES	LEED	EBMA	SIMS	ESCA	XDS	EHS IHS	ENS, INS
Probe Emitted particle	$h\nu$ $\bar{e}$	γ $\bar{e}$	$\bar{e}$ $\bar{e}$	$\bar{e}$ $\bar{e}$	$\bar{e}$ γ	I I	$\bar{e}$ $h\nu$	γ $\bar{e}$	He	n
Analysed areas, mm^2	5	5	$5\cdot10^{-8}$	5	1	3–10	1–50	1–50	1–50	10^6
Lateral resolution, nm	$\sim10^3$	10^2–10^3	<0.1	<0.05	0.5–10	<1	0.1	10^{-2}–10^{-3}	20	100
Depth resolution, nm	0.5–5	0.5–5	0.5–5	0.5–5	$>1\cdot10^4$	>0.3	1–10^2	0.5–5	0.3	≥0.3
Detectable amount of substance, at.%	0.1	0.1	0.1	0.1	0.1	<0.001	0.1	0.1	<0.001	<0.001
ditto, g cm^{-2}	10^{-10}	10^{-10}	10^{-10}	10^{-10}	10^{-10}	10^{-13}	10^{-10}	10^{-10}	10^{-13}	10^{-13}

Symbols. I, ions; γ, X-ray quanta; $\bar{e}$, electrons; $h\nu$, light quanta; n, neutrons; He, helium atoms.

process) cannot be re-established without changing the nature of the solution.

A description of the effect of the roughness (or curvature) of the surface K_M on the chemical activity of its different regions is implicit in the well known Gibbs–Thomson equation, according to which the difference $\Delta\mu$ between the chemical potentials of the particles in the solid located on a projection or in a groove is proportional to the curvature K_M of the surface:

$$\Delta\mu = \gamma^0_{ij}\Omega K_M.$$

The curvature can be defined as

$$K_M \simeq d^2y/dx^2$$

where x, y are the coordinates. For $x \to 0$ the difference $\Delta\mu$ is a maximum, and therefore atoms tend to be transferred from projections to the flat surface. In this way the surface tension γ^0_{ij} of the crystal grain can minimise its surface area.

The kinetics of the dissolution of M are described by the Arrhenius expression[13]

$$i = k\theta\exp(-E_a/RT),$$

where k is the rate constant, θ is the coverage of the surface by the products of the dissolution reaction E_a is the activation energy of the dissolution, R is the gas constant, and T is the absolute temperature. In practice the ratio of the rates of dissolution (i) on portions of the surface of types r and s is the most useful parameter. The rate of dissolution of projections (i_p) on the M surface is greater than the rate of dissolution of hollows (i_h). If the projections and the hollows are approximated by hemispheres of atomic dimensions ($\sim$0.01 nm) the ratio of i_p to i_h can be written

$$i_p/i_h = \exp(2\gamma^0_{ij}\Omega/R_S RT), \quad (5)$$

where $R_S = K_M^{-1}$ is the radius of curvature of the surface ($R_S > 0$ for a projection, $R_S < 0$ for a hollow).

It has been pointed out[14] that hollows and projections (of curvature $K_{M,h}$ and $K_{M,p}$ respectively) will function as microanodes and microcathodes with a potential difference

$$\Delta E = (2\gamma^0_{ij}\Omega/zF)(K_{M,p} + K_{M,h}). \quad (6)$$

where F is the Faraday and z is the valency of the electrode reaction.

ΔE decreases with the square of the distance from the projection to the hollow, and the energy term (the dependence of ΔE on R_S) becomes a curve with a minimum at the distance $0.5\,R_S$.

For a flat boundary at $R_S \to \infty$ the Gibbs absorpton equation becomes

$$d\gamma^0_{ij} = -q_{S,0}dE_0 - \sum_i \Gamma_i d\mu_i\,, \quad (7)$$

where $q_{S,0}$ is the surface charge for an electrode potential E_0, $\Gamma_i = N_i/A_S$ is the number of adsorbed i particles (the Gibbs adsorption), N_i is the number of moles of the i-th component, and A_S is the surface area of the crystal. This equation cannot be used, since for T = const the system is invariant. However, when $K_M \neq 0$ we can write

$$d\gamma^0_{ij}/dR_S = -\Gamma_i(d\mu/dR_S) \quad (8)$$

and after some substitutions arrive at the Tolman equation[15]

$$\gamma^0_{ij}/\gamma^0_{ij\infty} = (1 + 2\delta/R_S)^{-1}\,. \quad (9)$$

For a flat surface $\delta/R_S \to 0$ and $\Gamma_i/\Delta\rho \to \delta$ (the distance from the interface); $\Delta\rho$ is the difference between the densities of the crystal and of the liquid phase. It is clear that the increase in Γ_i (i.e. the decrease in γ^0_{ij}) depends on the curvature of the corroding surface.

In a macroscopic analysis of the increments $\Delta\gamma^0_{ij}/\gamma^0_{ij}$ we must allow for a possible increase (as well as a decrease) in the surface area A_S. Gokhshtein[16] introduced the differential factor

$$\beta = \Delta A_S/A_S = \Delta\gamma^0_{ij}/\gamma^0_{ij},$$

related to the curvature of the surface K_M by the expression

$$\beta = 1/2[(1 - \nu)K_M + (1 + \nu)K_M^{-1},$$

where ν is the Poisson ratio for the metal ($\nu \cong 0.25$). The curvature of the surface K_M can be altered by the adsorption of species from the solution (with charge transfer) at the electrochemical contact. Faceting of the surface (to give S and K faces) is possible, including, as a first stage, the rearrangement of the near-surface layers of the crystal. The coherence of the coupling of the EDL with the metal and the electrolyte plays an essential role in the rearrangement of the first few surface layers of the crystal.

IV. Adsorption of chalcophilic particles and phase transitions of the second kind in the near-surface layers of monocrystals

An ideal crystal surface has the unique property of a stretched skin, i.e. an elastic surface tension γ_{ij} which compresses the inner part of the crystal. When a metallic crystal is cut to produce a new surface in transition metals, which contain electronic surface states of the Tamm or of the Shockley type, the atoms in the first near-surface layers are regrouped (rearranged, reconstructed), and γ_{ij} decreases. The radii of the first, second, and third coordination spheres on the newly formed surface of transition metals are greater than in the bulk (for example, for Fe the increase is $> 3\%$).

A strict thermodynamic description of the reconstruction of the near-surface layers can be based on Landau's theory of phase transitions.[17] Large displacements (Δd) of the atoms in the metal lattice are characterised by a nonlinear function for the deviation of the atoms from the given equilibrium positions (the nonlinear order parameter) in this theory. This function is exactly equivalent to a density wave in the metallic crystal.[18]

In the surface layers of very pure monocrystals the distance between the first and the second layer (Δd_{12}) at right angles to the surface is less than the corresponding distances in the bulk (Table 3), i.e. we observe a perturbation of the translational invariance and an alternation of the sign (with decreasing amplitude), which is more marked for the stepped nonsingular K faces [for example, (997), (991), (311), see Table 1]. This change in Δd, not related to the adsorption of particles from the solution, is a fundamental property of the first few near-surface layers of metallic crytals.

The reconstruction of the near-surface layer of a crystal was first described in terms of the charge model. The infringement of the translational invariance produces effectively localised electronic states

which give rise to surface energy bands from closely placed energy levels. The formation of surface charge and of an EDL of thickness comparable to that of the Debeye screening radius leads to the filling of the conduction band. An electric field normal to the surface and a bending of the energy bands are produced. A relaxation (a change in the displacement Δd) takes place under the influence of the surface tension forces, and the surface layer is reconstructed as a result of the difference in energy between the electronic states produced by small deformations of the surface structure. In diamond-like structures [for example, (111)Si] the relaxation can be as high as 30%.[19]

Table 3. Changes in the interplanar spacings of metals in the first near-surface layers, %.

(*hkl*)M	Δd_{12}	Δd_{23}	Δd_{34}	Refs.
(001)Ti	~ -2.0			[21]
(011)V	-0.3			
(001)V	-6.7	1.0		
(001)Fe	~ -1.5			
(211)Fe	-10.0	5.0		[20]
(310)Fe	-16.0	12.0	-4.0	
(001)Co	~ -4.0			
(111)Ni	-1.2±1.2			
(001)Ni	-3.2±0.5			[22]
(011)Ni	-8.7	3.0	-0.5	[20]
(011)Ni	-9.6	4.3		
(011)Ni	-4.8±1.6	2.4		
(011)Ni	-9.8±1.6	3.8±1.8		[22]
(011)Ni	-8.4	3.1		
(311)Ni	-15.9	4.1	-1.6	[20]
(111)Cu	-4.1±0.6	2.4		
(011)Cu	-7.9	2.3	-0.9	[21]
(011)Cu	-8.5	2.6		[20]
(011)Cu	-9.5			
(011)Cu	-10.0	3.3		
(001)Cu	~ -1.1			
(001)Mo	~ -11.5			[21]
(001)Mo	-9.5±2.0			
(110)Rh	-6.9±1.0	1.9±1.0		[23]
(011)Ag	~ -7.0±2.0	1.5	-2.0	
(011)Ag	~ -10.0			[21]
(011)Ag	-5.7	2.2		
(001)W	-2.0			[24]
(001)W	~ -6.0			[20]
(011)Re	-17.0	1.0		[21]
(111)Al	0.9			[20]
(111)Al	~ 5.0			
(111)Al	2.2	5.5	+2.2	
(011)Al	-8.5	5.2±0.2	-1.6	[21]
(011)Al	~ -10.0			
(011)Al	~ -4.0			
(311)Al	-13.0	9.0		[24]
(311)Al	-11.7±2.3	-4.1±3.1	10.3±2.7	[25]

During the reconstruction of the surface layers of the crystal we observe transverse and longitudinal displacements in the first rows of atoms in addition to the displacements Δd normal to the surface. Transverse relaxation is found on singular, low-index F faces, such as the (111), (110), and (100) faces of b.c.c. crystals of the transition metals. Both longitudinal and transverse displacements of the atoms in the first layers of atoms are possible on nonsingular S faces [for example (210), (310), and (211)].[20]

The compressive stresses in the first near-surface layers of crystals are always replaced in the deeper layers by compensating expansion stresses produced by the action of the *sp* electron gas and by the short-range repulsive pair interactions between the atoms. The tangential displacements (Δd_r) of the atoms in the first layers are expressed[26] as

$$\Delta d_r = -\frac{1}{2G_c}\int_0^\infty f_1(tr)[\nu t^2\varphi + (1-\nu)\frac{\partial^2\varphi}{\partial z^2}]dt, \qquad (10)$$

where G_c is Young's modulus, φ and r are the spherical coordinates, f_1 is a Bessel function, and the z axis is directed towards the bulk of the crystal.

A test of formula (10) by computer calculations shows that these stresses have a variable sign. The adsorption of particles from the solution produces a rearrangement which stabilises the surface layer: a phase transition of the second kind takes place in a thin layer of the crystal. Obviously, two mechanisms can be suggested for the effect of adsorbed SAS on the reconstruction of the surface:[27] (*i*) in some metals the symmetry of the atomic arrangement is modified by the adsorption of SAS, approaching the symmetry found in the bulk, and (*ii*) the adsorption of the SAS produces a reconstruction of the surface which stabilises it. These are usually the least close packed F faces in the f.c.c. (011) and the b.c.c. lattices [(001) and (111)].

According to Benneman and Tomanek[28] the reconstruction of the surface is the result of the minimisation of the surface free energy (which at $T = 0$ K is the half-sum of E_b for the two free surfaces) associated with the surface tension:

$$\gamma_{ij}^0 = \frac{1}{N_S}\sum_{i=1}^{N_A}(E_{b,k} - E_{b,i}), \qquad (11)$$

where $E_{b,k}$ and $E_{b,i}$ are the binding energies of the atoms in the bulk and on the surface of the crystal, and N_A is Avogadro's number. Acording to Rusanov[29] the tangential forces Δd_r act in a near-surface layer of thickness l, and therefore Eqn. (11) should be re-written

$$\gamma_{ij}^0 = \int_0^l(\sigma(z) - \sigma^0)dz,$$

where $\sigma(z)$ and σ^0 are the stress tensors in the bulk and on the surface of the crystal.

The heat of reconstruction of the clean surface $\Delta\gamma_R^0$ is the difference between the surface tensions of the rearranged (γ_R^0) and the nonrearranged surfaces (γ_u^0):

$$\Delta\gamma_R^0 = \gamma_R^0 - \gamma_u^0. \qquad (12)$$

The changes in d produced by the reconstruction of the surface are entirely different in the presence of an adsorbed SAS. There are a few crystals whose clean surfaces do not become reconstructed, and also some crystals in which the amplitude of the atomic vibrations in the first layers is comparable with the amplitude of the vibration of the adsorbed SAS particles, and the rearrangement proceeds as a cooperative resonance process. When SAS species are adsorbed the heat of reconstruction [according to (12)] becomes:

$$\Delta\gamma_R = \Delta\gamma_R^0 - \Delta\gamma_{ads}. \qquad (13)$$

In this expression

$$\Delta\gamma_{ads} = \theta_{SAS}(E_{ads,R} - E_{ads,u}), \quad (14)$$

where E_{ads} is the energy of the adsorbate–adsorbent bond and the difference $E_{ads,R} - E_{ads,u}$ is determined by calculation or experimentally. From Eqn (14) we obtain the main diagnostic criterion for the supression or the initiation of the reconstruction:

$$\Delta\gamma_R = \Delta\gamma_R^0 - \Delta\gamma_{ads} < 0, \quad (15)$$

which can be determined by a simple method (Fig. 3).

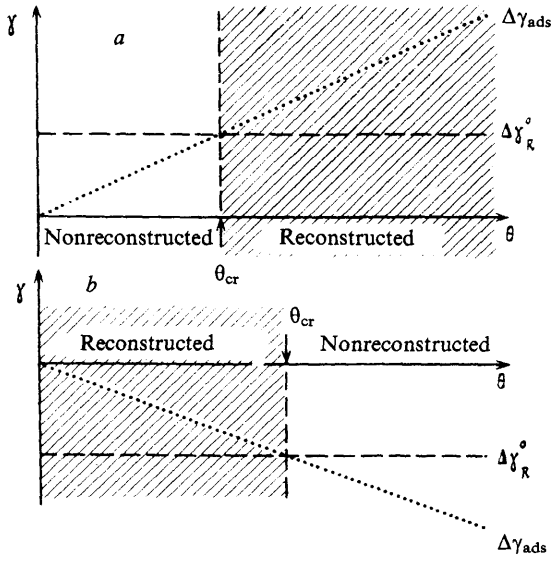


Figure 3. Changes in surface energy during the reconstruction of the near-surface layer of the metal:[24] *a*, onset of reconstruction; *b*, suppression of reconstruction.

In order to obtain the surface tension γ_{ij}^0 by Eqn. (11) we must expand $E_{b,i}$ into two terms:

$$E_L(x) = \Delta E_{rep}(z) + \Delta E_b(z), \quad (16)$$

where $\Delta E_{rep}(z)$ is the Born–Mayer phenomenological short-range repulsive potential: $\Delta E_{rep} = \Sigma A_S exp(-pR_{a,i})$, $R_{a,i}$ is the length of the bond along the z axis between the adsorbed particle and the M(i) surface atom, p is the damping coefficint, and $\Delta E_b(z)$ is the contribution from the adsorbate–adsorbent interaction. Eqn. (16) shows that the driving forces of the rearrangement are the elastic forces in the near-surface layer. The rearrangement induces a change in the chemical composition of alloys. A LEED study of the enrichment of the first surface layer in the close-packed (111) face of a monocrystal of the $Pt_{0.1}Ni_{0.9}$ alloy by platinum atoms[30] showed that the degree of enrichment can reach 30 ± 4% while the second layer is depleted of platinum by 5 ± 3%. Therefore we must allow for the ennobling of the surface even before the contact with the electrolyte when calculating the corrosion resistance of binary alloys containing a noble metal component. The ennobling of the surface layer is a well known phenomenon in corrosion or anodic dissolution studies, but it is usually attributed to the transport of alloy components into the solution and their subsequent reprecipitation.

In electrochemical dissolution processes of M taking place at low speed the rearrangement of the surface layer is undoubtedly an active factor. The ionisation of the metal during dissolution $M^0 \rightarrow M^{+n} + ne^-$, produced by the breaking of the M–M bond followed by charge transfer, should lead to periodic pulsations of the atoms in the first layer associated with the formation of metastable states. This effect will be reflected in the magnitude of the current flowing through the electrochemical system. Instability of the surface structure is mainly seen in the *d* metals with a half-filled *d* band. The mechanical instability (reconstruction) stimulates a rearrangement of the force and energy distributions on the surface, leading to electrical instability.

This type of electrical instability, accompanied by current pulsations (oscillations), is often observed in electrochemical processes on solid electrodes under conditions of pre-phase (adsorptional) evolution of material on the surface at relatively low overvoltages (η = 0.02–0.03 V) in the cathodic or the anodic region. Current oscillations may result in periodic mechanical vibrations in the M/electrolyte system, whose amplitude depends on the shape of the electrode and on the electrolysis parameters.[31]

V. Reconstruction of monocrystal surfaces during the adsorption of hydrogen, oxygen, and halogens

The adsorption of light chalcophilic species (hydrogen, oxygen, haloens) produces the highest activity in the reconstruction of the near-surface layers of metals.

Hydrogen

An analysis of the interaction of hydrogen with the near-surface layers of transition metal monocrystals is of practical value in the chemistry of catalysis and in the assessment of corrosion and brittleness in constructional materials. The reversible absorption of hydrogen in a metal plays an important role in hydrogen energetics. We shall discuss the structural effects resulting from the adsorption of hydrogen on the surface of the transition metals of Groups IB, VIB, and VIII of the Periodic Table, beginning with the adsorption of hydrogen from the gas phase, because this information is invariably used in the analysis of the contact between a metal and an electrolyte. The studies were carried out by LEED, AES, IRS, and other methods.

Adsorption from the gas phase. Most of the experimental work was done with well characterised nickel monocrystal surfaces. The adsorption parameters depend on (*hkl*), but it has been shown that the nickel (100) and (111) faces are affected similarly by the adsorption of hydrogen.[22] There are two sequentially filled β states, with activation energies for desorption of ~0.84 (β_1) and 1.00 eV (β_2). The number of hydrogen atoms in the adsorbed monolayer (*ML*) varies between $\sim 3 \times 10^{18}$ and 1.5×10^{19} atoms m^{-2}, i.e. it is slightly lower than N_S for these faces. The work function of the electron (Φ_M) from the surface of the metal M increases in proportion to the filling of the nickel surface by hydrogen (θ_H) up to saturation (state β_2), reaching ~0.2 eV at saturation (θ_H = 1 *ML*,

5×10^{-2} Pa, 298 K). LEED measurements indicate the formation of a disordered adsorbed layer of hydrogen on nickel at 298 K.

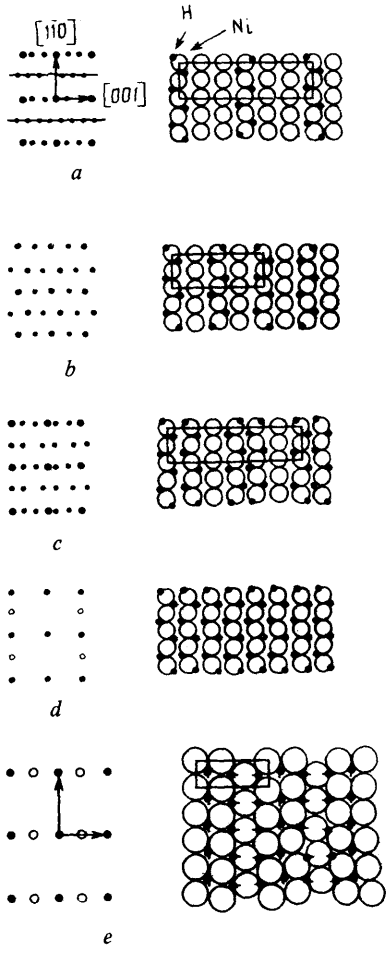


Figure 4. Superstructures formed on the (110)Ni face for different θ_H (*ML*): *a*, 0.33; *b*, 0.50; *c*, 0.67; *d*, 1.00; *e*, 1.50; on the left, LEED diffraction pattern, on the right, model.[32]

The adsorption of hydrogen on the least close packed (110) face of nickel shows some special features.[32–35] In particular, it has been shown that at the θ_H values for which $\Phi_m \cong 0.06$ eV a one-dimensional structure with the same periodicity (1×2) as the nickel lattice is formed as a result of the attraction of the adsorbed hydrogen atoms in the [1$\bar{1}$0] direction along the rows of nickel atoms of the first near-surface layer. This phase transition of the second kind is accompanied by an increase in the binding energy of the hydrogen to the nickel E_{Ni-H}, but the interactions of the adsorbed atoms in the [001] direction, across the above rows, are much weaker. The periodicity of the structures produced by the adsorption are strongly dependent on θ_H:[32] at $\theta_H = 0.33$ *ML* the first disordered (2×6) superstructure is formed, the (2×4) superstructure at $\theta_H = 0.5$ *ML*, a second (2×6) at $\theta_H = 0.67$ *ML*, and at still higher coverages we find the (2×1)–2H at $\theta_H = 1.0$ *ML* and finally the (1×2)–3H at $\theta_H = 1.5$ *ML* (i.e. at saturation) (Fig. 4). Hydrogenation of the (110) nickel face ($T \geqslant 220$ K) produces "stripes" with a (1×2)–3H structure in the [001] direction. The surface is reconstructed and consists of paired and of extended rows of nickel atoms. The hydrogen aotms are adsorbed on two (*r* and *s*) positions with a low and a high Ni–H bond energy respectively,[33] i.e. in the triple vacancies between the first two nickel layers parallel to the paired rows of the first layer in the [1$\bar{1}$0] direction, forming saw-like chains, and in the triple vacancies normal to the rows of nickel atoms in the [001] direction. The length of the Ni–H bond becomes 1.72 ± 0.01 nm, and the nickel atoms of the second layer are displaced alternately and mutually at right angles by ± 0.02 nm. The density of the adsorbed hydrogen atoms is 1.71×10^{19} atoms m^{-2}, and $E_{Ni-h} \simeq 2.75$ eV. There are reports[34,35] that at $T = 298$ K the chemisorption of hydrogen on (110)Ni–(1×1)H rearranges the surface into (110)Ni–(5×2)H, so that the nickel atoms of the first layer are shifted by 0.05 nm in the direction of dimerisation (Fig. 5), forming tetramers, which can also be interpreted as a combination of paired and extended rows (every fifth row in the [001] direction is extended).

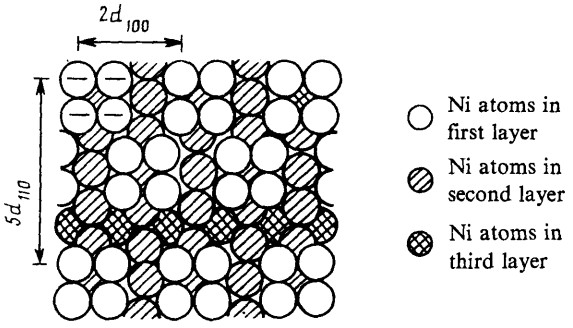


Figure 5. (5×2) Superstructure formed on (110)Ni by the adsorption of 0.5 *ML* of hydrogen at $T = 298$ K.[34]

In the high-index nickel *S* faces [for example, (997)Ni, (510)Ni, etc.] the presence of steps and terraces plays an important role, as was pointed out above. Thus, on the (510)Ni face at $T \simeq 100$K and coverages up to $\theta_H \leqslant 0.9$ *ML* hydrogen is adsorbed both on the terraces and on the steps (with preferential coverage of the steps),[36] and at $\theta_H > 0.9$ *ML* even molecular hydrogen is adsorbed, but only on the step edges.

The stepped (997)Ni *S* face, which is a combination of monoatomic (111) steps and nine-atom (111) terraces (Table 1), has a hydrogen capture probability at $T = 298$ K 10 times higher than the singular (111)Ni *F* face.[37] At low temperatures ($T \leqslant 250$ K) hydrogen adsorption takes place mainly on the step edges, but at high temperatures it extends over the terraces (according to LEED and HEED studies). The predominant adsorption of hydrogen on the steps can be demonstrated by the dependence of the sticking coefficient on the angle of incidence (Fig. 6). We can see that at $T = 90$ K the function $s_0(\theta_H)$ is determined exclusively by the presence of steps. Conversely, at $T = 800$ K only the terraces affect the kinetics of adsorption, and the plot of the $s_0(\theta_H)$ function is identical to that obtained for the (111) plane, inclined at 6.4° to the (997) plane.

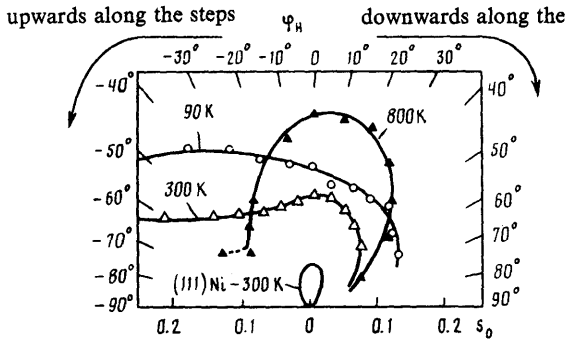


Figure 6. Dependence of the sticking coefficient s_0 on the angle of incidence of the molecular beam of hydrogen φ_H on the (997) and (111) nickel faces at different temperatures.[36]

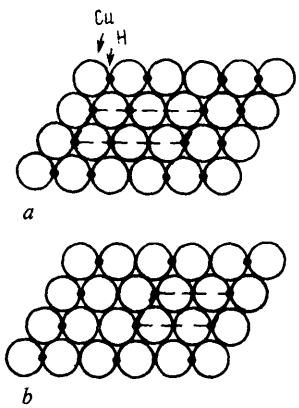


Figure 7. Superstructures formed on the (111)Cu face:[39] *a*, (3 × 1); *b*, (2 × 1).

Copper

On the (110)Cu face the adsorption of hydrogen is mainly in the atomic form,[32] with low values of E_a (0.18–0.20 eV), denoting a low probability of attachment of hydrogen molecules. It has been shown by LEED measurements that subsurface reconstruction with formation of a specific (1 ×2)* phase takes place at 300 K. The octahedral surface position of the hydrogen atoms is more favourable than the interstitial position in the bulk of the metal, but it is less stable (by 0.3 eV) than the normal chemisorption position.[38] Under these conditions a substantial contribution to the stabilisation is provided by the change in the relaxation of the near-surface layer of atoms (Δd_{12} = 4–9.6% at θ_h = 0.5 *ML*). Of course, so far we have no definite model of the resulting structure, because of the difficulty of correlating the LEED results variously obtained for the (110)Cu surface covered with hydrogen.

A study of the temperature dependence of the adsorption of hydrogen on the (111)Cu surface by IR spectroscopy has shown[39] the presence of two superstructures (3 × 3) at 150 K and (2 × 2), into which the (3 × 3) phase is converted when heated to 186 K (Fig. 7). The structures are combinations of domains with (3 × 1) and (2 × 1) orientations. The adsorbed hydrogen atoms are accommodated in (111)Cu double vacancies parallel to the rows, so that every third row is extended for the (3 × 1) structure and every second for the (2 × 1) structure. The filling with hydrogen of the double vacancies is confirmed by studies of the electron energy loss spectra (ν_1 = 1040 cm^{-1}, whereas a ν_1 frequency of 1000 cm^{-1} is calculated for the filling of triple vacancies).

Ruthenium

Like the (110)Ni–H system, the (100)Ru–H system forms a wide spectrum of superstructures at low temperatures, depending on θ_H. At θ_H = 2.0 *ML* we find the (1 × 1)–2H structure (Fig. 8), in which the chains of adsorbed hydrogen atoms are arranged only in the [$\bar{1}$20] direction, unlike the (1 × 2) structure obtained for nickel.[32] A reversible surface reconstruction takes place at θ_H = 1.5 *ML*: in this state alternate ruthenium atoms are raised above the plane of the surface, and form a (2 × 2) structure. The density of adsorbed hydrogen atoms at θ_H = 2.0 *ML* is 1.73 × 10^{19} atoms m^{-2}, with E_{Ru-h} = 2.7 eV, which is comparable with the N–H bond energy. According to the desorption spectra hydrogen can be adsorbed in the α_1, β_1, and β_3 states, which exist at 220, 260, and 350 K respectively. The α_1 state corresponds to the formation of a (1 × 1)–2h structure (θ_H = 2.0 *ML*), the β_1 (probably) to the formation of a (2 × 2) structure (θ_H = 1.5 *ML*), and the β_3 state to the (1 × 2) structure. As in the case of nickel the sticking coefficient s_0 initially has very high values ($s_0 \simeq 1$), so that a coverage of only 0.3–0.4 *ML* of hydrogen is sufficient to saturate this state. However, s_0 rapidly falls to ~0.1 for the filling of the β_1 state at θ_H = 1.5 *ML*, and the rate of adsorption also falls.

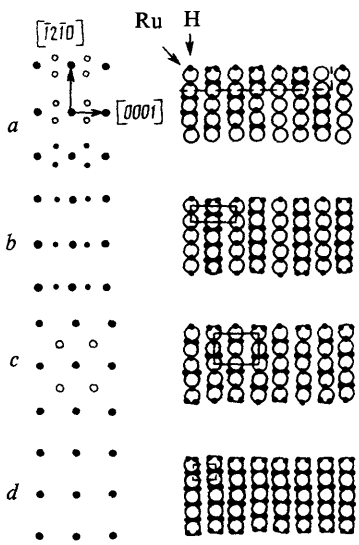


Figure 8. Superstructures formed on the (100)Ru face for different θ_H (*ML*):[32] *a*, 1.0; *b*, 1.4; *c*, 1.5; *d*, 2.0.

Rhodium

The structures obtained in the adsorption of hydrogen on the (110)Rh face (Fig. 9) are similar to those found on ruthenium.[32] At θ_H = 2.0 *ML* a structure with a periodicity of (1 × 1) is formed,

with two hydrogen atoms in the unit cell. The hydrogen occupies triple vacancies, forming linear chains in the [1$\bar{1}$0] direction, but in this arrangement it produces stronger changes in the surface relaxation of the rhodium atoms than it does in ruthenium.[40] As in other *d* metals, we find a compression at right angles to the surface (a decrease in Δd, Table 3). The distance between the layers is 0.132 nm, and the length of the Rh–H bond is 0.184 nm.

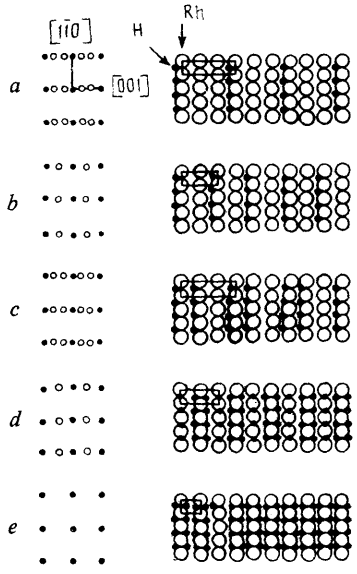


Figure 9. Superstructures formed on the (110)Rh face for different θ_H (*ML*):[32] *a*, 0.33; *b*, 0.50; *c*, 0.67; *d*, 1.60; *e*, 2.00.

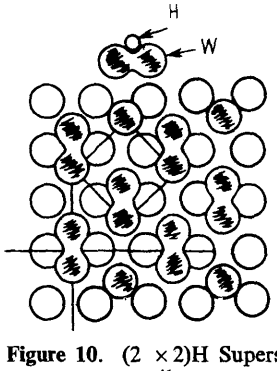


Figure 10. (2 × 2)H Superstructure formed on the (100)W face for θ_H = 0.25 *ML*.[41]

Under these conditions the density of the hydrogen atoms is ~2 × 10^{19} atoms m^{-2}. The high bond energy E_{Rh-H} = 5.7 eV [unlike E_{Ni-H} = 2.7 eV for (110)Ni] can account for the lack of surface reconstruction in rhodium even after the adsorption of large amounts of hydrogen. The hydrogen desorption spectra show that two states are being filled: α_1 (at 138 K), corresponding to the (1 × 1)–2H structure (θ_H = 2.0 *ML*), and α_2 ($T \simeq$ 250 K), corresponding to the (1 × 2) structure (θ_H = 1.5 *ML*). As was subsequently pointed out,[25] at θ_H = 0.5 *ML* a reconstruction takes place, yielding a (1 × 2)–2H structure in which the hydrogen atoms occupy three-coordinated positions between two atoms of the upper layer and one atom of the second layer, and are arranged along rows of rhodium atoms in the [1$\bar{1}$0] direction. The surface relaxation changes so as to maintain a distance of 0.127 nm between the first and the second layer, which is comparable with the results obtained for the (1 × 1) structure. The electronic work function Φ_M reaches 0.930 eV for $\theta_H \to 1$ *ML*, but the increase in Φ_H is not affected by an increase in p_{H_2}.[42] This effect is attributed[42] to the preferred orientation of the hydrogen dipole with its negative end towards the gas phase.

Tungsten

At $T \simeq$ 300 K and low surface coverages of the (100)W surface flash desorption reveals one adsorbed β_2 state whose formation is completed at θ_H = 0.16–0.25 *ML*. At higher surface loadings we observe a second (β_1) state in which the density of adsorbate is 2.0 × 10^{18} molecules m^{-2}.[22] The ratio of the concentrations corresponding to saturation in each of the states is σ_1/σ_2 = 2. The adsorption of hydrogen in the β_1 state producs a diffraction pattern corresponding to the (2 × 2) structure, which reduces to the ordered (1 × 1) structure at θ_H = 1 *ML* (Fig. 10), with molecules and atoms accommodated in tetrapores. The adsorption of hydrogen on the (100)W *F* face at θ_H < 0.25 *ML* produces a reconstruction with the surface tungsten atoms in pairs in the [100] direction, forming dimers, and the adsorbed hydrogen atoms are accommodated on the surface atoms as saw-tooth chains.[41]

Flash desorption studies of the (100) and (110) tungsten faces gave similar results.[22] When the adsorption has taken place at 300 K we observe two peaks for β_1 and β_2 states with E_{W-H} bond energies of 1.2 and 1.4 eV respectively. When saturated these states contain approximately the same number of particles, formed by dissociative adsorption; at θ_H = 0.5 *ML*, when the β_2 state is filled, a (2 × 1) structure is formed and the hydrogen is again accommodated in tetrapores. the density of adsorbate in the β_2 state is 1.42 × 10^{19} atoms m^{-2}. The electronic work function decreases with increasing coverage during the adsorption in this state, reaching Φ_M = 0–(–0.5) eV at θ_H = 1.0 *ML*. There are reports that multilayer coverage (θ_H = 8 *ML*, 300 K) produces a reconstruction of the less closely packed (110)W face in which the tungsten atoms are shifted relative to each other in a [1$\bar{1}$0] direction and the hydrogen atoms occupy triple vacancies.[43]

In the b.c.c. tungsten lattice the (211)W is the simplest *S* face, containing atoms having two coordinations: in close-packed rows, forming the first or the surface layer respectively, or in the channels between rows.[9] Though the latter are in the second layer they are accessible to adsorption. This nonuniformity of the face is reflected by the hydrogen adsorption. We observe two adsorption states, β_1 and β_2, which are filled sequentially at $T \simeq$ 100 K. They correspond to atomic states with approximately equal contents of adsorbate at saturation. The sticking probability is $s_0 \simeq 1$, and the decrease in s_0 produced by an increase in Φ_H is proportional to $(1-\theta_H)$. The LEED method failed to detect the formation of a structure with a (1 × 1) periodicity. The electronic work function Φ_M increases by ~0.6 eV for β_2 but falls when the β_1 state is filled. This is explained by the structual properties of the (211)W face towards the adsorbed hydrogen (the adsorbed β_1 state is above the

plane of the surface, and the β_2 state is below it). If a hydrogen atom is adsorbed in a β_1 state (in the uppermost close-packed rows) its dipole is oriented with its positive end towards the metal, resulting in a decrease of Φ_M.

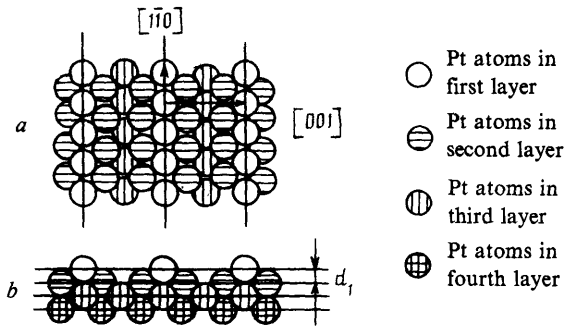


Figure 11. (110)−(1 × 2)Pt Superstructure formed after treating the (110)Pt surface in ultra-high vacuum:[32] *a*, plan view; *b*, side view.

Platinum

As we know, the clean surface of the "loose" (110)Pt face (unlike that of nickel or rhodium) is unstable and is spontaneously reconstructed into a (1 × 2) structure when treated in a high vacuum, so that each row is extended in the [001] direction.[32] In this way the third layer of platinum atoms becomes accessible to the adsorption of hydrogen as well as the second. The surface of the (110)Pt face can be represented as an assembly of (110) micro-facets inclined at 109.5° relative to each other, containing various types of triple or double vacancies between the first and the second layer. The hydrogen adsorbed on these sites does not affect the initial reconstruction (Fig. 11). Of course, the faceted (110)Pt surface is relatively rough and therefore can hold more hydrogen atoms than other faces [$\theta_H = (2.2 \pm 0.2) \times 10^{19}$ atoms m^{-2}]. The hydrogen is adsorbed in two states [β_1 and β_2, for $\theta_H = (0.4-0.6)$ *ML*, 300 K].

The β_1 state formed at $T \simeq 200$ K requires longer exposures to reach saturation. Initially the sticking probability is $s_0 \simeq 1$, but during the filling of the β_1 state $s_0 = 0.022$ and $E_{Pt-H} \simeq 2.8$ eV. The electronic work function initially increases with the coverage ($\Phi_M = 0.170$ eV for $\theta_H = 0.3$ *ML*), but at $\theta_H = 1$ *ML* Φ_M falls to 0.05 eV (Fig. 12). This is explained by the difference between the dipole moments of the β_1 and the β_2 state ($\mu_2 = +0.12$ D for β_2 and $\mu_1 = -0.17$ D for β_1, where 1 D = 10^{-2} C m[44]), which depend on the topology of the adsorbed hydrogen. The filling of the β_1 state corresponds to the adsorption of hydrogen on the (111) micro-facets, when the negative ends of the dipoles of the hydrogen adatoms are directed towards the upper row of platinum atoms. The adatoms themselves lie below the plane of the image charge, i.e. in the triple vacancies, and this lowers the dipole moment of the metal.

Two adsorption states have been observed by the thermal desorption of hydrogen from the close packed (111)Pt face, but at 300 K the β_1 state is absent because of the low energy of the Pt−H bond, and the β_2 state is only partially filled.[9] It has been shown that in the β_1 and the β_2 state the hydrogen is atomically bound to the platinum and that at $\theta_H = 1$ *ML* the amounts of these two states are approximately equal. The hydrogen is adsorbed in triple vacancies between the atoms of the first and the second platinum layer without perturbing the ordered (1 × 1) structure, so that the length of the Pt−H bond is 0.058 nm,[45,46] and $E_{Pt-H} \simeq 2.6$ eV.

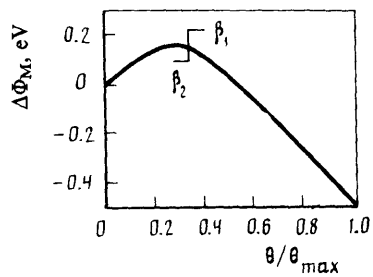


Figure 12. Dependence of the electronic work function Φ_M on the surface coverage θ_H for the (110)Pt face;[44] β_1 and β_2 are the adsorption states.

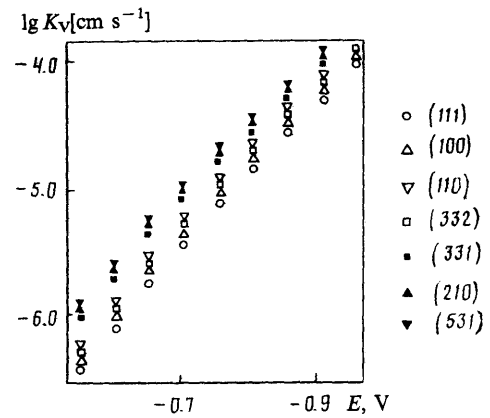


Figure 13. Dependence of the rate of the hydrogen evolution reaction on the potential for different *F* and *S* faces of a gold monocrystal (0.1 M $HClO_4$).[47]

Interesting results have been obtained on the stepped (997)Pt face [a combination of monoatomic steps and nine-atom terraces, oriented in the [111] direction]. As on the (997)Ni face, the sticking probability s_0 was found to be very high [~4 times greater than on the singular (111)Pt face.[32,34]]. At high coverages $\theta \geqslant ML$ the s_0 values for (997)Pt (like the Φ_M values) are comparable with those obtained for (111)Ni. However, at low saturations the "loose" steps of the (997)Pt *S* face act as centres on which the hydrogen is adsorbed most rapidly, is held most strongly, and has a dipole of opposite sign to that of hydrogen adsorbed on (111)Pt. There is evidence of the presence of a second break in the dependence of s_0 and $\Delta\Phi_M$ on θ_H at $\theta_H = 0.15$ *ML*: 9 hydrogen atoms are adsorbed

on each terrace at saturation. Therefore the two centres at the ends of each terrace have a stronger Pt–H bond energy than the others, and are the first to be filled. It is experimentally established that these centres are geometrically different from the others, and that the hydrogen atoms adsorbed on them have dipoles different from the rest.

Adsorption in solutions of electrolytes

The adsorption of electrochemically reduced hydrogen (during which the pressure of the gas on the metal surface is much higher than p_{H_2} = 1 GPa) has been adequately studied on well characterised faces of gold, platinum, nickel, and niobium monocrystals.[47–60]

Thus the hydrogen evolution reaction (HER) has been studied not only on the low-index gold faces, but also on the (311), (210), (332), and (531) *S* faces, consisting of sets of steps and terraces.[47] It was found that both in $HClO_4$ solutions and in electrolytes with specifically adsorbed halogen ions (Hal^- = F^-, Cl^-, Br^-, I^-) the HER is slower on the close-packed faces, but faster when the faces contain steps and breaks. The rate of the HER increased with the concentration β_0 of monoatomic steps; for example, in a solution of NaF the rate of the HER on the (210) gold face was ~3.5 times higher than on the (111) face (Fig. 13). This is due mainly to the decrease of Φ_M on the atomically rough *S* and *K* faces. Obviously, the low-coordinated *r* states on the crystal surface have a catalytic effect on the adsorption of hydrogen. When in contact with the surface the hydrogen fills the tetrapores on the steps, forming bonds.

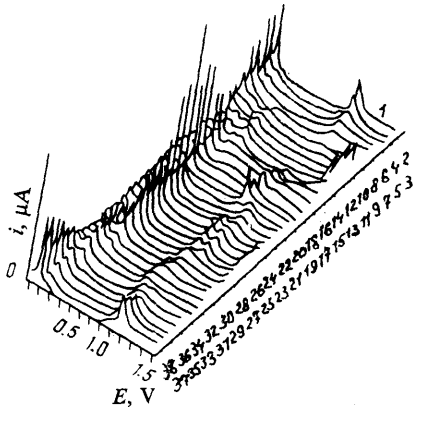


Figure 14. Current–voltage diagrams for Pt faces of different crystalline orientation.[49] Face indices: *1*, (110); *2*, (551); *3*, (331); *4*, (227); *5*, (332); *6*, (554); *7*, (10109); *8*, (202019); *9*, (111); *10*, (201919); *11*, (1099); *12*, (544); *13*, (355); *14*, (322); *15*, (513); *16*, (211); *17*, (311); *18*, (511); *19*, (211); *20*, (911); *21*, (1711); *22*, (3111); *23*, (100); *24*, (2110); *25*, (1510); *26*, (1210); *27*, (910); *28*, (610); *29*, (510); *30*, (410); *31*, (310); *32*, (210); *33*, (530); *34*, (320); *35*, (430); *36*, (620); *37*, (12110); *38*, (110).

These pores offer strong bond positions (*s* state) which are energetically more favourable to adsorption. The difference in E_{M-H} energies between the weakly bound (*r*) and the strongly bound states (*s*) is determined essentially by the crystallographic parameters of the hydrogen adsorption. This has been experimentally demonstrated, for example, for the (881), (771), and (661) *k* faces of an Fe + 3% Si crystal,[48] which are combinations of 8-, 7-, and 6-atom terraces, consisting of (110) planes and of loose monoatomic (100) steps. The radii of the tetrapores (*s* state) on the (110)Fe and (100)Fe faces are r_{110} = 0.00173 and r_{100} = 0.0766 nm. Therefore, since the radius of a hydrogen atom is r_h = 0.046 nm, the adsorbed hydrogen can easily penetrate into the pores in the steps afer being discharged, but the process is suppressed in the close-packed terraces.

The form of the cyclic potentiodynamic potential–current curves depends on the density of β_0 and (*hkl*) steps in the platinum *S* faces.[49] As β_0 decreases, i.e. as the packing density S_{hkl} is increased, the characteristic hydrogen adsorption peak moves into the region of positive potentials (Fig. 14), due to the increase in Φ_M and to the corresponding shift of the zero charge potential $E_{q=0}$. it can also be seen that, as the less densely packed steps become saturated, hydrogen begins to be evolved on the terraces and the intensity of the corresponding peak is increased. Cyclic potentiodynamic curves can be used for a quantitative as well as a qualitative assessment of the adsorption on the *K* faces of monocrytals, and in particular for determining the structural characteristics of these faces, as was demonstrated[50] for the [*n*(111) × (100)] platinum surfaces (*n* = 2–9, 12, 14, 20, 26, and 40).

High-sensitivity optical methods[51] are now widely used to determine the changes in structure of monocrystal surface at the contact with electrolytes. We know that the form of the electroreflectance (ER) spectra depends on the crystallographic orientation of the faces; the $\Delta R/R$ effect (where *R* is the Fresnel reflection coefficient) is smaller when the lattice is most closely packd [for an f.c.c. lattice, of copper (say), the sharpest peaks are found in the spectrum of the (311) *S* faces, and the weakest in the spectrum of the (111) face[52]]. Furthermore the presence of steps and of terraces with different crystallographic orientations is also reflected by the shape of the spectral lines.

The structure of the interface between monocrystalline gold [(111), (100), (110), and (210) faces] or silver electrodes [(111) and (100) faces] and an aqueous solution of 0.01 M NaF has been studied ellipsometrically.[53] As before, a strong dependence of the optical spectra near $E_{q=0}$ on the crystallographic orientation of the electrodes was noted [though the spectra of the reconstructed and of the nonreconstructed (100)Au faces do not differ very markedly]. The effect of the charge density *q* on the polarisation angle Δ depends on the sign of the charge; for $q < 0$ only a small $q = f(\Delta)$ response is observed. This is consistent with the assumption of a weak metal–solvent interaction. The sharp change in the level of the optical signals for $q > 0$, largely determined by the crystallographic orientation of the sample, can be attributed to the onset of specific adsorption of the anions and to a strong $M-H_2O$ interaction. Information on the surface structure was obtained by calculating the relaxation time of the free electrons τ: the greater is τ, the smaller is the difference in structure between the surface and the bulk. As expected, the highest value of τ was found for the most closely packed (111)Au face.

Subsurface defects (dislocations, vacancies, and their combinations) have a marked influence on the electrochemical characteristics of a monocrystal suface. The walls of the etch pits formed on defects can be described as a combination of terraces (*F* faces) and steps with breaks (*k* faces). This produces new adsorption–desorption peaks, not seen on the potential–current curves of well ordered surfaces of perfect monocrystals.[54] The application of a relatively small number of oxidation–reduction

cycles, or of a high-temperature anneal, eliminates the defect portions of the electrochemical process and finally yields an improved potential–current curve.

However, it hs been reported[55] that extending the range of applied potentials can produce irreversible changes in the potential–current curve as a result of a far-reaching breakdown in the initial structure of the metal. The same situation is found when the scan rate of the potential is increased (>0.1 V s^{-1}); fast cycling "strikes" the metal atoms in the near-surface layer from their equilibrium positions. This results in microfaceting, i.e. in a change in surface structure accompanied by the formation of highly coordinated adsorption s states. Fig. 15 shows, as an example, the cyclic potentiodynamic E, i curves for the (111)Au and (111)Pt faces for different scan rates and different ranges of the applied potential. The structure of the (111)Pt and (100)Pt surfaces has been studied by transmission electron microscopy (TEM) after various cycles of electrochemical treatment.[56,57]

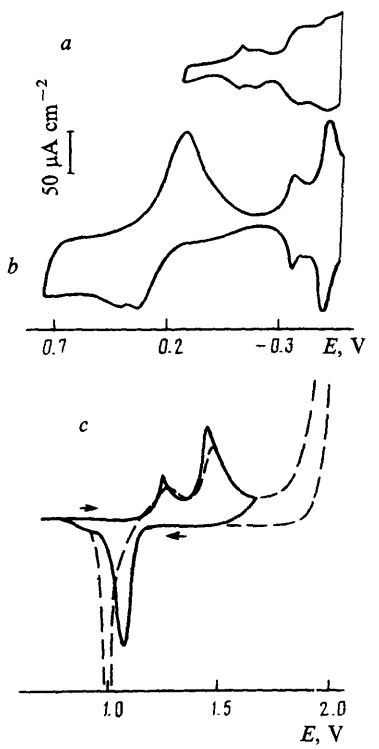


Figure 15. Current–voltage curves of the (111)Pt and (111)Au faces for different potential scan rates and different applied potentials: *a*, (111)Pt, 0.5 M H_2SO_4, V_E = 0.5 V s^{-1}, E = 0.15–(–0.48) V; *b* (111)Pt, 0.5 M H_2SO_4, V_E = 0.2 v s^{-1}, E = 0.70–(–0.5) V;[58] *c*, (111)Au, 0.1 M $HClO_4$, V_E = 0.02 V s^{-1}, E = 0.7–1.7 V (full line), E = 0.7–2.0 V (broken line).[93]

Let us examine more closely the electrochemical faceting process. The (111)Pt and (100)Pt faces were subjected to the so-called (100) treatment in a solution of 0.5 M H_2SO_4, consisting in the application of rectangular potential pulses (0.23–1.23 V) at a frequency of 3.5 kHz. Under these conditions the potential E varied cyclically between the hydrogen evolution region and the oxide formation region (–0.5–0.7 V) for a short time (0.5–5 s). This treatment had a radical influence on the morphology of the (111)Pt face [while the (100)Pt face was not significantly affected], and the results were comparable with the application of several hundred single pulses of the potential. After 5 s of this treatment the (111)Pt face showed an increased roughness K_M, the steps became flat and well defined, and the outline of the terraces was markedly altered by the formation of K faces (with atomic projections and hollows), seen in the TEM pictures as small kinks on the terrace surfaces. The monocrystallinity of the (111)Pt steps after the electrochemical treatment is explained by the ability of the steps to act as recesses for Pt adatoms, leading to cluster formation and thus being self-perpetuating. After 50 cycles of applied potential (0.77–0.53 V) with a scan rate of 0.2 V s^{-1} less than 10% of the surface has escaped the phase transition of the second kind (faceting).[58] In this case the shape of the E, i curve is similar to that obtained for polycrystalline platinum. Thus the parameters of the electrochemical treatment (E and V_E values, frequency of the applied pulses, etc.) have a strong influence on the morphology and on the crystallographic orientation of the experimenal faces. These effects explain the large differences in the published results.[59]

In the electrochemical reactions, as in the adsorption of hydrogen from the gas phase, the surface of metal monocrystals becomes reconstructed.[60] Homa, et al.[61] described the transition of the (100)–(5 × 20)Pt structure into the (100)–(1 × 1)Pt structure after contact with the 0.1 M HF + CO electrolyte while cycling E between 0.05 and 0.50 V or without an applied potential. These workers conclude[61] that the instability of the surface is due to the adsorption of small quantities of CO during the preparation of the electrode for the experiment, which suppresses the reconstruction. The reverse transition from the (100)–(1 × 1)Pt to the (100)–(5 × 20)Pt structure during the contact of platinum monocrytals with 0.5 M H_2SO_4 + 0.1 M $H_2C_2O_4$ was observed by Orts, et al.[62] This reconstruction is typical not only of the (100)Pt surface but also of the (310), (610), and (211) platinum K faces, which contain terraces with a (100) orientation. As suggested,[62] the reconstruction process is due to the specific adsorption of the $HC_2O_4^-$ ions. There are reports[63] of the reconstruction of the (110)Pt surface at the contact with 1 M H_3PO_4 [transition of the (1 × 1) into the (1 × 2) superstructure by cycling E between 0.065 and 0.750 V with V_E = 0.05 s^{-1}]. The reconstruction of the (111)Au surface in a dilute solution of HF and $HClO_4$ has also been studied.[64] The (111)Au surface was pretreated in ultra-high vacuum by Ar^+ ion bombardment followed by heat treatment. The two-dimensional (111)–($\sqrt{3}$ × 22)Au structure, unstable at any applied potential, was formed on the close packed (111)Au surface. This was followed by the structural transition of (111)–($\sqrt{3}$ × 22)Au into the ordered (111)–(1 × 1)Au structure, which survived 10 cycles of potential scanning (0.2–1.75 V, V_E = 0.05 V s^{-1}).

Reports on the stability of the (100)Au face reconstructed by a similar vacuum treatment are contradictory. Thus, it was shown[52] that the resulting (100)–(5 × 20)Au structure (a hexagonal close packed upper layer on a square sublattice) is stabilised by immersion in 0.01 M solutions of $HClO_4$ and H_2SO_4 over the whole range of applied potential, which excludes specific adsorption (up to 0.31 V in $HClO_4$ and up to 0.11 V in H_2SO_4). This reconstruction is suppressed only by the adsorption of ClO_4^- and SO_4^{2-} anions. However, other works[64,65] find that the (100)–(5 × 20)Au structure, like the (111)–($\sqrt{3}$ × 22)Au structure, is converted into the

ordered (111)−(1 × 1)Au structure at any applied poential. The difference in surface tension $\Delta\gamma_{ij}$ between these structures is only 0.06−0.09 eV, and therefore a phase transition of the second kind can take place even in the physisorption region with $E_b \simeq 0.1$ eV. The stability of the (100)−(5 × 20)Au structure in contact with an electrolyte is attributed[65] to contamination of the surface during the preparation of the gold monocrystals by silicon and alkali metals, which stabilise the reconstructed surfaces of the 3*d* transition elements.

The (110)Au surface is reconstructed after being annealed and cleaned in an ultra-high vacuum. It forms a (1 × 2) superstructure which survive cyclic changes in potential (−0.35−0.45 V) when immersed in 0.01 M $HClO_4$. Contamination of the clean (110)Au surface by small quantities of calcium induced the formation of a (1 × 3) structure, which was again transformed into a (1 × 2) structure by the application of a variable potential in the same electrolyte.[66] This is inconsistent with Hamelin's results.[65]

The reconstruction of the (100)Au face in 0.005 M H_2SO_4 during cyclic changes in E (−0.1−1.3 V) was studied by electroreflectance spectroscopy.[67] The difference between the optical spectra of reconstructed and of nonreconstructed surfaces was attributed[67] to the presence of surface Tamm states, suppressed by the adsorption of SAS during phase transitions of the second kind. From the increase (or decease) in the height of the characteristic peaks for the optical transitions from the *d* band to the empty surface states in the ER spectrum the kinetics of the reconstruction of the (100)Au face were determined.

Oxygen

In an electrochemical corrosion process it is important to allow for the surface relaxation of the oxygen adsorbed on the metal surface, which has a high chemical affinity for the transition metals. The chemisorption of oxygen (like the chemisorption of halide ions) at 298−2300 k increases the distance between the uppermost near-surface layers: $\Delta d_{12} = 2.0 \pm 1.0\%$ in the case of the $p(2 \times 2)$ surface structure observed for coverages $\theta_0 < 0.4$ *ML*, and $\Delta d_{12} = 5.2 \pm 1.5\%$ in the case of the $c(2 \times 2)$ for 0.4 *ML* $< \theta_0 <$ 0.46 *ML* (*p* and *c* refer to the cell types: *p* for primitive and *c* for centred). The particles adsorbed from the solution usually stabilise (freeze) both the normal and the tangential vibrations of the atoms in the surface layer of the metal.

The study of these vibrations was begun by Germer, et al.,[68] who examined the "loose" (110)Ni faces. In the first two layers the amplitudes of the vibrations in the mutually perpendicular <001> and <110> directions differed by a factor of ~1.5, and in the deeper layer (beyond the sixth) the amplitudes were comparable. The amplitude of the vibration of the surface layers normal to the surface (0.0117−0.0001 nm) is much greater than the amplitude of the atomic vibrations in the bulk (0.0080 nm); this ratio of the amplitudes, which is very important in corrosion studies, is not affected by the adsorption of oxygen. An important structural feature of the oxidation is the negligibly small effect of the relaxation of the surface layer of the crystal on the Coulombic barrier opposing the penetration of the adsorbed oxygen into the metal. Thus, for the (111)Cu face Bauschicher[69] showed that the reconstruction of the near-surface layer, which begins after the adsorption of the first three oxygen atoms (at $\theta_0 = 0.5$ *ML*), lowers the energy barrier to the penetration of additional oxygen atoms from 8.2 to 5.3 eV. This process initiates the reconstruction of the surface, since the chemical bond for the incorporation of additional oxygen atoms is strengthened.[70]

The reconstruction of the low-index faces of monocrystals as θ_0 is increased has long been recognised.[71] The work function Φ_M increases at first during the adsorption of the first portions of oxygen on the (001)Ni surface, and then decreases (due to the reconstruction of the first layer of the crystal). The kinetics of the reconstruction of the (2 × 4) into the (2 × 1) structure on the (011)Ni face during the adsorption of oxygen are described by the well known Avrami−Kolmogorov equation, which assumes an initial induction period:

$$V_t/V = 1 - \exp(-K_t t^m), \tag{17}$$

where V and V_t are the rate of reconstruction of the surface without and with oxygen respectively, K_t and m are coefficients and $m \simeq 0.3$. The height of the activation energy barrier is 0.23 eV. On the (001)Ni and (011)Ni faces the charge transfer from the nickel to the oxygen atoms increases with θ_0, and the energy of the Ni−O bond decreases,[70] as does also the number of holes in the 3*d* sub-band (as a result of the hybridisation of the 3*d* states of nickel and of the 2*p* states of the adsorbed oxygen).[72] The "fit" of the oxygen on the ideal surface of the *F* crystal face is improved by a decrease in Φ_M (and therefore also in S_{hkl}).[73]

The adsorption of oxygen on the metal surface is followed by the formation of oxide (which usually has semiconductor properties). For layer thicknesses smaller than the Debye length $l_D = [2\varepsilon_{D,Ox}\varepsilon_{D,V}(\Phi_M - \Phi_{ox})/e^2 n_{Ox}]^{1/2}$ the band bending in the oxide (the shift by E_0 from the Fermi level E_F) is described by the equation[74]

$$E_F - E_C = E_{C0} \pm [en^2_{Ox}(\Phi_M - \Phi_{Ox})(l_{Ox} - l_D)2\varepsilon_{D,Ox}\varepsilon_{D,V}], \tag{18}$$

where Φ_{Ox} is the electronic work function of the oxide, l_{Ox} is the thickness of the oxide layer, $\bar{n}_{Ox}$ is the average concentration of free electrons in the oxide, E_C is the energy of the bottom of the conduction band, E_{C_0} is the position of the bottom of the conduction band of the oxide for $l_{ox} > l_D$; $\varepsilon_{D,Ox}$ is the dielectric permittivity of the medium and $\varepsilon_{D,C}$ is the dielectric permittivity of free space ($\varepsilon_V = 8.854 \times 10^{-12}$ F m^{-1}). According to Eqn. (18) $E_F - E_C$ varies as the oxide thickness l_{ox} increases. The surface energy E_C is determined by the ratio of Φ_m to Φ_{Ox}, decreasing steeply at first when the adsorption layer of oxygen is formed and then stabilising as l_{ox} continues to increase. A decrease in γ^0_{ij} [and therefore also in ΔE, see Eqn. (6)] suppresses the electrochemical dissolution of the metal.

The ionic conductivity of the oxide films is exponentially dependent on the electric field within the oxide E_{Ox}, and can be calculated by the Günterschultz−Betz equation

$$i_+ = A_+ \exp(B_+ E_{Ox}), \tag{19}$$

where A_+ and B_+ are empirical constants of dimensions A m^{-2} and m V^{-1} respectively. The formation of these films on the *d* metals is made possible by the reconstruction of the first few layers of the crystals. Thus, in the $p(2 \times 2)0/(111)$Ni surface structure the length of the Ni−Ni bonds is increased by ~1.5 nm (sic., Ed. of Translation),[75] which helps the fitting of the next portions of oxygen and their clustering. According to LEED and AES data[76] at surface coverages of the (001)Ni surface by adsorbed oxygen $\theta_0 \leqslant 0.25$ *ML* ($T = 500$ K) we observe a $p(2 \times 2)$ structure, at 0.25 *ML* $\leqslant \theta_0 \leqslant$ 0.35 *ML* a $c(2 \times 2)$ as well as the $p(2 \times 20$ structure, and at $\theta_0 \geqslant$ 0.35 *ML* only the $c(2 \times 2)$ structure. Reiudle, et al.[76] assume that a $p(1 \times 1)$ structure is also possible. The most stable is the $p(2 \times 2)$

structure, in which the oxygen atom is in a highly coordinated state in the tetrapore.

In the least densely packed (110)Ni plane (as shown by some early experiments[77]) the oxygen successively forms the (3 × 1), (2 × 1), and (3 × 1) surface structures at $\theta_0 \leqslant 0.3$ *ML*. The oxygen occupies long bridging positions in a strongly coordinated state with a 3 nm Ni–O distance, forming rows in the [001] direction (Fig. 16). A decrease in the activation energy of 0.03–0.05 eV (at θ_0 = 0.5 *ML*) is produced by the rearrangement (faceting) of only the first three near-surface layers (Fig. 16*d*).

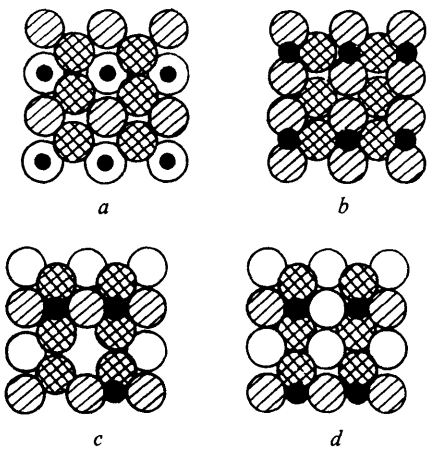


Figure 16. Structure of the (2 × 1) oxygen adsorption phase on the (110)Ni face: *a*, weakly coordinated adsorption of oxygen without reconstruction of the near-surface layer; *b*, reconstruction of the face through the replacement of Ni by O atoms; *c*, reconstruction of the face with displacement of the Ni atoms; *d*, faceting of the face during the adsorption of O ("tooth separation" model[77]).

Comparing the chemical compositions of oxygen layers prepared from the gas phase (10^{-4} Pa, 500 nm) and by electrochemical oxidation at a constant potential *E* (0.01 M $HClO_4$, 1.05 V) shows that in the latter case the NiO layer (l_{Ox} = 85 nm) is covered with a hydroxide layer (l_{HOx} = 25 nm).[78] The structures of the oxide layers are also different: the (100)NiO face is formed from the gas phase and a disordered phase with local inclusions of (111)NiO from the electrolyte.

The energy of the M–O bond is quite high (4.0–14.0 eV), and the dissolution of the oxide at the corrosion potential E_{cor} in pure water according to Purbaix' data[79] seems thermodynamically improbable for many *d* metals. The breakdown of the oxide in aqueous media is accompanied by the penetration of anions (A^-) into the oxide with simultaneous adsorption of water molecules. Some comments by Vijh on these processes[80] are based on the relative values of the dielectric constants of water (ε_{D,H_2O}) and of the oxide ($\varepsilon_{D,Ox}$), and of the electric fields E_{H_2O}, E_{ox}. For an anodic potential of 1 V a field $E_V = 10^{10}\,\varepsilon_{D,V}$ V m^{-1} normal to the electrode surface is produced, in a vacuum, in an oxide layer 10 nm thick.

Table 4. Dielectric constants of the oxides.

Oxide	$10^8 E_{Ox}$, V m^{-1}	ε_{Ox}	$10^{10} D$, V m^{-1}	$10^3(1/\varepsilon_{Ox})$	l_D, nm
Bi_2O_3	2.2	40	0.88	25.0	30.0
UO_3	3.6	25(UO_2)	0.90	40.0	11.9
Y_2O_3	4.4	18	0.79	55.5	23.9
Nb_2O_5	4.6	41	1.92	24.1	11.8
ZrO_2	5.1	22–25	1.02–1.35	40.0	16.0
TiO_2	5.0	15–40	0.75–2.00	25.0	6.4
WO_3	5.5	42(WO_2)	2.31	23.8	5.5
Ta_2O_5	6.2	27	1.71	36.2	7.3
Al_2O_3	7.9	8–10	6.32–8.29	95.2	12.7
SiO_2	26.0	3	0.91	285.7	4.2

In an aqueous solution (unlike a vacuum) we must allow for the adsorption of water and for the formation of an electrical double layer. The normal field at the anode–electrolyte contact is $E_{H_2O} = E_V/\varepsilon_{D,H_2O}$; for an anodic oxide it is $E_{ox} = E_V/\varepsilon_{D,Ox}$. Therefore we can write $E_V = E_{H_2O}\varepsilon_{D,H_2O} = E_{Ox}\varepsilon_{D,Ox} = 1 \times 10^{10}$ V m^{-1} and characterise the changes in the oxide in terms of the dielectric displacement vector. Indeed, for many oxides we find that $E_V \equiv D$ = const (Table 4). By using the universal constant *D* we can explain the formation of thick layers on the valve metals and of thin layers on the noble metals. The width of the tunnelling barrier l_D of the oxides is smaller in the metals which have a high chemical resistance. We can lower l_D and improve the electronic conductivity of the oxides of the valve metals (Nb, Ti, Zr) by anodic treatment in very concentrated alkaline solutions with anodic current densities $i_a = (2.5–4.0) \times 10^4$ A m^{-2}, E = 35 v, T = 303 K, t = 10–20 s.[81]

The thermodynamic description of the simultaneous adsorption of A^- anions and of water molecules on the metal surface:

$$A^-(H_2O)_n + (H_2O)_{ads}(M) \rightleftarrows A^-(M) + (H_2O)_{n+1},$$

requires a knowledge of the hydrophilicity or hydrophobicity ΔG°_{hydr} of the adsorbent.[82] The change in Gibbs free energy is

$$\Delta G^\circ_{ads} = \Delta G^\circ_{hydr} + \Delta G^\circ_{M-A^-} - \Delta G^\circ_{M-H_2O}, \qquad (20)$$

where $\Delta G^\circ_{M-A^-}$ and $\Delta G^\circ_{M-H_2O}$ are the parts of the free energy responsible for the adsorption of the anion and of water, and $\Delta G^\circ_{hydr} = \Delta G^\circ_{A^- - H_2O}$ is the chemical energy of hydration of the anion. According to Trasatti's calculations[82] the linear increase in the zero-charge potential $E_{q=0}$ with increasing reticular density of

the monocrystal surface S_{hkl} is responsible for a decrease in ΔG°_{ads}. For two corroding metals in contact with the solution Eqn. (20) becomes

$$\Delta(\Delta G^\circ_{ads}) = -\Delta(\Delta G^\circ_{M-H_2O}). \quad (21)$$

Halide ions

Experimental determinations of ΔG° have been carried out for systems composed of halide ions and well characterised low-index faces of noble metals.[83] Depending on the reticular density S_{hkl} the values of the second term in Eqn. (20) can be arranged in the sequence

$$-\Delta G^\circ[(111)M\text{–}Hal^-] > -\Delta G^\circ[(001)M\text{–}Hal^-] > -\Delta G^\circ[(011)M\text{–}Hal^-].$$

The specifically adsorbed Hal^- anions weaken the bond in the $M-H_2O$ complex. In crystals with a covalent bond and *s, p* metals (Cd, Sn, Bi) the relationship (21) was tested by studying the adsorption of aliphatic alcohols,[84] assuming that the interactions of $R-OH$ (where $R \equiv nCH_2$ denotes the methyl groups in the SAS) with the surface are negligible (for $nCH_2 = 0$, $\Delta G^\circ = 0$), i.e. the change in free energy per methyl group should be zero. The ability of the SAS to become adsorbed on two corroding metals in ohmic contact (often met in practice) is determined by the properties of the water in the EDL and in the bulk of the solution:

$$\frac{\Delta(\Delta G^\circ_0)}{\Delta n} = \frac{\Delta(\Delta G_S)}{\Delta n} - \frac{\Delta(\Delta G_V)}{\Delta n}. \quad (22)$$

The change in the energy of hydrophobic hydration in the bulk (ΔG_V) and in the EDL (ΔG_S) for aliphatic alcohols, calculated by Eqn (21), shows that the contribution of the interaction energy of the water molecules to the energy of adsorpion is insignificant and approximately the same for different *s, p* metals.[84]

Water on a metal surface has a low-entropy structure; the entropy factor is determined by the (*hkl*) of the surface. In the case of chemisorbed halide ions incorporated in the interstitial sites between the surface metal atoms the energy term is characterised, as for $H_{ads}(M)$ and $O_{ads}(M)$, by two maxima, i.e. we have states of strong and of weak specific adsorption. It is believed that the transfer of charge from the halide ion to the metal is accompanied by a change in the orientation of the water molecules in the $Hal(H_2O)^-_6$ cluster being discharged (from the orientation with the oxygen atoms towards the surface to the orientation with the hydrogen atoms towards the surface[85]). The formation of adsorption cluster structures on the metal surface strengthens the charge transfer as compared with the single atom: the charge transfer coefficient (the Esin–Markov coefficient K_{EM}) is greater for the cluster than for the single Hal atom.

In the strong specific adsorption the Hal^- ion is accommodated in a many-centre adsorption site on the metal surface, but if the adsorption is weak and the transfer of charge is only partial the reconstruction of the hydration shell of the ion is not substantial. Crystallographic factors have a large influence on the standard thermodynamic parameters of the adsorption of halide ions. On platinum electrodes, and on electrodes of the other *d* metals, we observe an increase in the entropy of adsorpion and a decrease in the Gibbs free energy and in the enthalpy. The standard thermodynamic parameters for the adsorption of Cl^- ions on Pt and on Hg (kJ mol^{-1}) are:[86]

	ΔG	ΔH	$T\Delta S$
Hg	–2.06	–10	7.9
Pt	–6.10	–30	23.8

The "charging" of the metal surface by halide ions suppresses the formation of passivating oxygen compound: the thickness of the passivating layer l_{Ox} decreases with increasing concentration c_{Hal^-} in the solution and with increasing time of immersion of the electrode in the medium containing halogen. The halide ions can be arranged in the following series with respect to their effectiveness in the dissolution of the 3*d* transition metals: $F^- > Cl^- > Br^- > I^-$. The electrically negative halide ions adsorbed on the metal surface weaken the $d-\pi^*$ interaction with the passivating chalcophilic particles, and they assist the desorption of adsorbed hydrogen from the surface of the transition metals. The desorbing action of the halide ions can be adequately explained in terms of formal kinetics. For the Volmer–Heyrovsky mechanism of the hydrogen evolution reaction (HER), realised as two consecutive one-electron transfers to the M_k active centres:

$$H_9O_4^+ + M_k + e^- \rightarrow M_kH_{ads} + 4H_2O, \quad (23)$$

$$M_kH_{ads} + H_9O_4^+ + e^- \rightarrow M_k + 4H_2O + H_2, \quad (24)$$

the conjugated competing process

$$Hal^- + M_k \rightarrow M_kHal_{ads} + e^-, \quad (25)$$

$$M_kHal_{ads} + Hal^- \rightarrow M_k + Hal_2 + e^-, \quad (26)$$

leads to the generation of very mobile charge carriers which are free to tunnel. Reactions (23)–(26) on metal surfaces completely or partially covered with an oxide phase improve the electronic conduction in the solid phase and lower the chemical resistance of the metal.

Data on the coherence of the contacting phases and on the structure of halogen ad-layers on the well characterised surfaces of noble-metal monocrystals have been obtained in recent years.

Platinum

Structural studies by LEED and AES methods of the (111)Pt face in contact with aqueous solutions of KBr or $CaBr_2$ at different pH have shown that the adsorbed halide ion forms an ordered (111)Pt–(3 × 3)Br structure on the metal surface,[87] similar to the structure obtained by exposing platinum to HBr vapour in a vacuum.[88] This structure can exist at positive potentials, but it is reconstructed by the incipient reduction (with desorption) of the bromine atoms at –0.1 V by the scheme

$$(111)Pt\text{–}(3\times3)Br[\theta_{Br} = 4/9ML] + $$

$$+ xe^- \rightleftarrows (111)Pt(4\times4)[\theta_{Br} = 7/16ML] + xBr^-,$$

where x corresponds to only $4/9 - 7/16 = 0.007$ electron per Br^- anion on one surface Pt atom. This means that the adsorption of bromide (like that of other halide ions) is a redox process with partial charge transfer. The adsorption of halide ions is more marked in acid solutions than in alkaline solutions, mainly because

of the competition with adsorbates containing oxygen [see Eqn. (20)], which interact strongly with the surface. The ordered (1 × 1) structure and the diffuse oxygen surface layer with $\theta_0 = 0.5$ *ML* are retained during the initial stages of oxidation of the platinum, but in the second stage (as was pointed out above) the ordering is perturbed in both the platinum and the oxygen.

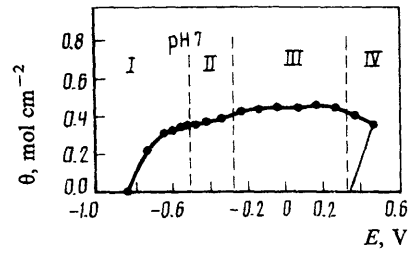


Figure 17. Dependence of the packing density of the iodine atoms on the (111)Pt face upon the electrode potential:[87] *I*, region of existence of the $(\sqrt{3} \times \sqrt{3})R30°-I$ superstructure; *II*, region of simultaneous existence of the $(\sqrt{3} \times \sqrt{3})R30°-I$ and $(\sqrt{7} \times \sqrt{7})R19°-I$ superstructures; *III*, region of existence of the $(\sqrt{7} \times \sqrt{7})R19°-I$ superstructure; *IV*, region of existence of the $(3 \times 3)-I$ superstructure.

Immersing the (111)Pt face in aqueous solutions containing iodine produces an ordered ad-layer of iodine atoms[87] whose packing density and structure depend on the potential (Fig. 17). The (111)Pt−(3 × 3)I[θ_I = 4.9 *ML*] structure exists at moderately high positive potentials (~0.5 V), the (111)Pt−$(\sqrt{7} \times \sqrt{7})R19°-$I[$\theta_i$ = 3/7 *ML*] at intermediate potentials (~0.1 V), and the (111)Pt−$(\sqrt{3} \times \sqrt{3})R30°-$I[$\theta_I$ = 1/3 *ML*] at negative potentials (< −0.5 V).

The reductive desorption of I^- anions takes place at very high negative potentials (< −0.8 V). All these structures are observed also after treating (111)Pt with HI and I_2 vapour in a vacuum.[89] The adsorption of iodine vapour on the stepped [6(111) × (111)]Pt(*s*) platinum surface failed to reveal even a partial affinity of the iodine atoms for the stepped formations on the surface.[90] Instead, the presence of steps (kinks) produced several phase domains with a local (3 × 3) or $(\sqrt{3} \times \sqrt{3})R30°$ geometry, and a structural correspondence of the adjoining terraces [6(111) × (111)]Pt−(3 × 1*T*)−I, [6(111) × (111)]Pt−(8 × 1*T*)−I, and [6(111) × (111)]Pt−(20 × 2*T*)−I.

As could have been expected, the chemosorption of chlorine anions on a platinum electrode is much weaker than the chemisorption of bromide or iodide. HCl species in a vacuum do not form an ordered layer on the (111)Pt face.[87] The peak on the *E*, *i* curve produced by the adsorption and desorption of chlorine can be distinguished from the hydrogen peak only because the former process [see reaction (25)] is independent of pH.[91] For $c_{HCl} \leqslant 0.01$ mol dm^{-3} the adsorption of chlorine becomes stronger, and produces an ordered (111)Pt−(3 × 3)Cl (τ_{Cl} = 0.33 *ML*) layer. The packing density of the chlorine is close to 0.5, which corresponds to the h.c.p. lattice.

Silver

The adsorption of halide ions on the (111)Ag face is an active process of the oxidation−reduction type,[87] as in the case of platinum. The reductive desorption of chlorine and bromine takes place almost entirely at negative potentials (< −0.8 V), and the iodine remains adsorbed over a wide range of potential (−0.6 to + 0.6 V). Chlorine and bromine atoms form simple (111)Ag−$(\sqrt{3} \times \sqrt{3})R30°-x$ structures, with θ_x = 1/3 *ML*, whereas iodine gives the structures which are also obtained in the electrodeposition of the silver on a (111)Pt face previously treated with iodine (Fig. 18). Thus the silver surface is reconstructed in solutions containing iodine.

Studies of the adsorption of halide ions by thermal desorption and UPS have shown that the adsorption−desorption characteristics are independent of the nature of the halogen.[92] Comparing the results for (110)Ag and (111)Ag confirms the strong topological dependence of the adsorpion of the halogens.

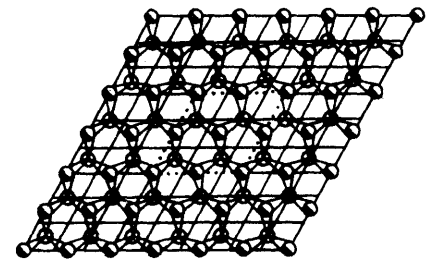


Figure 18. Structure of the (111)Pt−(3 × 3)Ag, I face; (θ_{Ag} = θ_I) = 4/9 *ML*.[87]

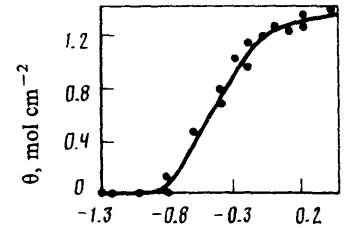


Figure 19. Dependence of the packing density of the bromine atoms on the (100)Au face upon the electrode potential.[93]

Gold

For the other noble metals only a few data on adsorption and surface reconstruction are available so far. The adsorption of bromine on the (100)Au face from aqueous solutions produces the (5 × 20)→(1 × 1) structural transition.[93] The dependence of the bromine packing density on the electrode potential (Fig. 19) can be described by the Avrami−Kolmogorov equation (17) with a long induction period and a potential < −0.5 V.

Copper

Chlorine adsorbed from a 10^{-3} M solution of HCl on the (100)Cu face forms the (100)Cu$-(\sqrt{2} \times \sqrt{2})R45°-$Cl structure with $\theta_{Cl} = 0.5$ *ML*, almost irrespective of the applied potential and of the concentration of chloride ions.[94] Desorption of the adsorbed chlorine is observed by immersing the electrode in 10^{-3} M H_2SO_4 at $E < -0.11$ V.

VI. Conclusions

Our analysis of the metastable states of the near-surface layer of metallic crystals in contact with a condensed (liquid) or a noncondensed (gas) medium suggests new approaches to corrosion-electrochemical processes (phase transitions of the first kind, accompanied by the evolution of adsorbed gases and by the adsorption and penetration of light chalcophilic species). Unique properties are found in the hydrogenated metal–electrolyte system. since hydrogen has an anomalously high diffusion coefficient in metals it is easly redistributed in the lattice and interacts with surface and subsurface defects, altering their concentration, topology, and energy state. Other outstanding aspects of the behaviour of hydrogen in condensed media are the ease with which it can lose (or gain) an electron, the ability of protons to generate heavier species dissolved in the metal, the contribution of H^- and H^+ to the deprotonation of adsorbed water structures, and the formation of new compounds in the adsorbed layers.

A new topic in electrochemistry has been created: the electrochemistry of monocrystals with well characterised surfaces. The possibility of analysing surface rearrangements by a whole group of high-resolution physical methods not only creates a new situation in this field of knowledge but also forces us to reconsider the traditional electrochemical approaches, which relied exclusively on an analysis of integral kinetic information on the transfer of charge across the metal–electrolyte interface

References

1. A A Lopatkin *Teoreticheskie Osnovy Fizicheskoi Adsorbtsii* (Theoretical Foundations of Physisorption), Izd. Moskov. Univ., 1983, 339 pp.
2. M Hentzer *Dynamic Phenomena on Surfaces, Interfaces, and Superlattices* (Proceedings of the International Summer School at Erice, July 1984), Berlin, 1985, p. 14
3. A Hamelin *Modern Aspects of Electrochemistry*, Plenum Press, New York, 1985, No. 16, p. 1
4. A Bartolini, F Ercolessi, E Tosatti *Helv. Phys. Acta*, 1989, **62** 820
5. J P Bourdin *J. Phys. F*, 1988, **18** 1801
6. P Horiuti *Z. Phys. Chem. (BRD)*, 1958, **15** 162
7. C T Campbell *Surf. Sci.*, 1986, **167** 181
8. V I Zubov *Zh. Fiz. Khim.*, 1988, **62**(4) 1026 [English translation in *Russ. J. Phys. Chem.*, 1988(4)]
9. E B Bezlepkina, Z V Kasatkin, V S Tsoi *Elektrokhimiya*, 1988, **24** 226
10. J Clavilier, D Armand, S G Sun, M J Petit *J. Electroanal. Chem.*, 1986, **205** 267
11. D Woodruff, T Delchar *Modern Methods of Studying Surfaces* (Translated into Russian), Mir, Moscow, 1989, 496 pp.
12. F N Chukhnovskii, V N Ol'tsev *Itogi Nauki i Tekhniki. Seriya Metallovedenie i Termicheskaya Obrabotka* (Advances in Science and Technology. Metal Science and Heat Treatment Series), VINITI, Moscow, 1988, Vol. 22, p. 125
13. V S Bagotskii *Osnovy Elektrokhimii* (Foundations of Electrochemistry), Khimiya, Moscow, 1988, 400 pp.
14. M Parlapanski *Proceedings of the Eleventh International Corrosion Congress*, Florence, April 1990, Vol. 3, p. 517
15. M Jaycock, J Parfitt *Chemistry of Interfaces* (Translated into Russian), Mir, Moscow, 1988, 400 pp.
16. A Ya Gokhshtein *Poverkhnostnoe Natyazhenie Tverdykh Tel i Adsorbtsiya* (The Surface Tension of Solids and Adsorption), Nauka, Moscow, 1976, 399 pp.
17. L D Landau, E M Lifshits *Statistichskaya Fizika* (Statistical Physics), Fizmatgiz, Moscow, 1967, 415 pp.
18. B Horovitz, R J Gooding, J A Krumhansl *Phys. Rev. Lett.*, 1989, **62** 843
19. J Bénard (Editor) *Adsorption on Metal Surfaces*, Elsevier, Amsterdam, 1983, p. 337
20. J S Luo, B Legrand *Phys. Rev. B*, 1988, **38** 1728
21. K Müller *Ber. Bunsenges. Phys. Chem.*, 1986, **90**(3) 184
22. M W Roberts, C S McKee *Chemistry of the Metal–Gas Interface* (Translated into Russian), Mir, Moscow, 1981, 539 pp.
23. W Ruchta, W Nichtl, W Oed, N Bickel *Phys. Rev. B*, 1989, **39** 1020
24. M Jo, M Onchi, M Nishjina *Surf. Sci.*, 1985, **154** 417
25. D L Adams, C S Sprensen *Surf. Sci.*, 1986, **166** 495
26. T V Berenshtein, A M D'yachenko *Ukr. Fiz. Khim.*, 1986, **31** 905
27. V P Zhdanov *Elementarnye Fiziko-khimicheskie Yavleniya na Poverkhnosti* (Elementary Physicochemicl Phenomena on Surfaces), Nauka, Moscow, 1989, 373 pp.
28. K H Benneman, D Tomanek *Phys. Rev. Lett.*, 1986, **5/7** 2594
29. A I Rusanov *Fazovye Ravnovesiya i Poverkhnostnye Yavleniya* (Phase Equilibria and Surface Phenomenon), Khimiya, Leningrad, 1967, 388 pp.
30. R Bandoing, Y Gauthier, M Lundberg, T Rundgren *J. Phys. C.: Solid Phys.*, 1986, **19** 2825
31. O Teschke, D M Soares, F Galembeck *J. Electrochem. Soc.*, 1985, **132** 1284
32. K Christmann *Mol. Phys.*, 1989, **66**(1) 1
33. B Voigtländer, S Lehwald, H Ibach *Surf. Sci.*, 1989, **208**(1/2) 1
34. Y Kuk, P J Silverman, H Q Nguyen *J. Vac. Sci. Technol. A*, 1988, **6**(3) Pt. 1 576
35. D A Harrington, P R Norton *J. Vac. Sci. Technol. A*, 1988, **6**(3) Pt. 1 778
36. A-S Martensson *Surf. Sci.*, 1989, **215**(1/2) 55
37. K D Rendulic *Appl. Phys. A*, 1988, **47**(1) 55
38. K W Jacobsen, J K Norskov *Phys. Rev. Lett.*, 1987, **59**(24) 2764
39. E M McCash, S F Parker, Jh Pritchard *Surf. Sci.*, 1989, **215**(3) 363
40. W Nichtle, N Bickel, L Hammer *Surf. Sci.*, 1987, **188**(8) 279
41. D King *Phys. World*, 1989, (3) 45
42. T V Kalish, M E Belyaeva, S I Sergeev *Elektrokhimiya*, 1987, **23**(1) 126
43. D Chauveau, C Guillot, B Villette *Solid State Commun.*, 1989, **69**(11) 1015
44. J R Engstron, W Tsai, W H Weinberg *J. Chem. Phys.*, 1987, **87** 3104

45. K Mortensen, F Besenbacher, I Stensgaard *Surf. Sci.*, 1989, **211–212** 813
46. P J Feibelman, D R Hamann *Surf. Sci.*, 1987, **182**(3) 411
47. A Hamelin *Modern Aspects of Electrochemistry*, Plenum Press, New York, 1985, No. 16, p. 123
48. G V Khaldeev, T F Borisova *Elektrokhimiya*, 1988, **24**(5) 618
49. N Furuya *Inf. Mater. Energy Theory Life*, 1988, **56**(3) 166
50. A Rodes, K Elachi, M A Zamakhchari, J Clavilier *J. Electroanal. Chem.*, 1990, **284**(1) 245
51. J E Fulghum, G E McGuire, L M Musselman, R J Nemanich *Anal. Chem.*, 1989, **61**(12) 243
52. D M Kolb *Phys. Chem.*, 1988, **92** 1175
53. F Chao, M Costa, J Lecoeur, J P Bellier *Electrochim. Acta*, 1989, **34**(12) 1627
54. E B Bezlepkina, Z V Kasatkin, V S Tsoi *Elektrokhimiya*, 1987, **23**(10) 1419
55. A Hamelin *Portug. Electochim. Acta*, 1987, **5** 77
56. D M Kolb *J. Vac. Sci. Technol.*, 1986, **4**(3) 1294
57. T Twomey, Y Uchida *Z. Phys. Chem. (BRD)*, 1988, **160**(1/2) 1
58. S Sugawara, K Itaya *J. Chem. Soc. Faraday Trans.*, 1989, **85**(6) Pt. 1 1351
59. A Visintin, J C Canullo, W E Triaca, A J Arvia *J. Electroanal. Chem.*, 1988, **239**(1/2) 67
60. A M Brodskii, L I Daikhin *Elektrokhimiya*, 1988, **23**(8) 1095
61. A S Homa, E Yeager, B Cahan *J. Electroanal. Chem.*, 1982, **150** 181
62. J M Orts, J M Feliu, A Aldaz, J Clavilier *J. Electroanal. Chem.*, 1990, **281**(1/2) 199
63. F Cases, E Morallon, J L Vazquez *Portug. Electrochim. Acta*, 1989, **7** 131
64. A T D'Agostino, P N Ross *Surf. Sci.*, 1987, **185**(1/2) 88
65. A Hamelin *J. Electroanal. Chem.*, 1988, **255**(1/2) 281
66. R Michaelis, D M Kolb *Surf. Sci.*, 1990, **234**(3) 281
67. D M Kolb, C Franke *Appl. Phys. A*, 1989, **49**(4) 379
68. A U McRae, L H Germer *Surf. Sci.*, 1964, **2** 522
69. Ch W Bauschicher *Chem. Phys. Lett.*, 1985, **118** 544
70. W Ravenek, F M M Geurts *J. Chem. Phys.*, 1986, **84** 1613
71. H Farnsworth *The Gas–Solid Interface* (Translated into Russian), Mir, Moscow, 1970, p. 359
72. A Seiter, C S Feigerle, I L Pena, R J Celotta *Phys. Rev. B.: Condensed Matter.*, 1985, **32** 7776
73. H Niehus, G Comsa *Surf. Sci.*, 1985, **151** 171
74. G P Peka *Fizicheskie Yavleniya na Poverkhnosti Poluprovodnikov* (Physical Phenomena on Semiconductor Surfaces), Vischcha Shkola, Kiev, 1984, 214 pp.
75. I S Caputi, S Holloway, I K Nirskov *Surf. Sci.*, 1986, **152/153** 660
76. S Reiudle, G M Pastor, K H Benneman *Surf. Sci.*, 1989, **211/212** 912
77. T Engel, K H Reider, I P Batra *Surf. Sci.*, 1984, **148** 321
78. F T Wagner, Th E Moylan *J. Electrochem. Sci.*, 1989, **136** 2498
79. M Pourbaix *Atlas d'EquilibresElectrochimiques*, Gauthier-Villars, Paris, 1963, p. 415
80. A K Vijh *React. Solids*, 1988, **4** 341
81. L P Bicelli, P Pedeferri, G Razzini *Int. J. Hydrogen Energy*, 1986, **11** 647
82. S Trasatti *Electrochim. Acta*, 1983, **28** 1083
83. G Valette *J. Electroanal. Chem.*, 1988, **255** 215
84. F I Danilov, V I Grishchuk, S A Panasenko *Ukr. Khim. Zh. (Russ. Ed.)*, 1989, **55** 830
85. A M Kusnetsov, R R Nazmutdinov, M S Shapnik *Elektrokhimiya*, 986, **22** 836
86. S Minc, M Jurkiewicz-Herbich *J. Electroanal. Chem.*, 1972, **34** 351
87. A T Hubbard *Chem. Rev.*, 1988, **88**(4) 633
88. G A Garwood, A T Hubbard *Surf. Sci.*, 1982, **112** 281
89. F Lu, G N Salaita, X Baltruschat, A T Hubbard *J. Electroanal. Chem. Interfacial Electrochem.*, 1987, **222** 305
90. A Wieckowski, B C Schardt, S D Rosasco, J L Stickney *Surf. Sci.*, 1984, **146** 115
91. T Solomun, A Wieckowski, S D Rosasco, A T Hubbard *Surf. Sci.*, 1984, **147** 211
92. H Hinzert, K K Kleinherbers, E Janssen, A Goldmann *Appl. Phys. A*, 1989, **49** 313
93. D Trevor, C E D Chidsey, D N Loiacono *Phys. Rev. Lett.*, 1989, **62** 929
94. C B Elers, I Villegas, J L Stickney *J. Electroanal. Chem.*, 1990, **284**(2) 403